Membrane lipid organization and nicotinic acetylcholine receptor function: A two-way physiological relationship

C. Fabiani [a], V.N. Georgiev [b], D.A. Peñalva [a], L. Sigaut [c], L. Pietrasanta [c,d], J. Corradi [a], R. Dimova [b], S.S. Antollini [a,*]

[a] Instituto de Investigaciones Bioquímicas de Bahía Blanca CONICET-UNS, Departamento de Biología, Bioquímica y Farmacia, Universidad Nacional del Sur, Bahía Blanca, Argentina
[b] Max Planck Institute of Colloids and Interfaces, Science Park Golm, Potsdam, 14476, Germany
[c] Departamento de Física, Instituto de Física de Buenos Aires (IFIBA), CONICET-UBA, Facultad de Ciencias Exactas y Naturales, Universidad de Buenos Aires, Buenos Aires, Argentina
[d] Centro de Microscopías Avanzadas, Facultad de Ciencias Exactas y Naturales, Universidad de Buenos Aires, Buenos Aires, Argentina

ARTICLE INFO

ABSTRACT

Nicotinic acetylcholine receptors (nAChRs) are involved in a great range of physiological and pathological conditions. Since they are transmembrane proteins, they interact strongly with the lipids surrounding them. Thus, the plasma membrane composition and heterogeneity play an essential role for the correct nAChR function, on the one hand, and the nAChR influences its immediate lipid environment, on the other hand. The aim of this work was to investigate in more detail the role of the biophysical properties of the membrane in nAChR function and vice versa, focusing on the relationship between Chol and nAChRs. To this end, we worked with different model systems which were treated either with (i) more Chol, (ii) cholesteryl hemisuccinate, or (iii) the enzyme cholesterol oxidase to generate different membrane sterol conditions and in the absence and presence of γTM4 peptide as a representative model of the nAChR.

Fluorescence measurements with crystal violet and patch-clamp recordings were used to study nAChR conformation and function, respectively. Using confocal microscopy of giant unilamellar vesicles we probed the membrane phase state/order and organization (coexistence of lipid domains) and lipid-nAChR interaction. Our results show a feedback relationship between membrane organization and nAChR function, i.e. whereas the presence of a model of nAChRs conditions membrane organization, changing its lipid microenvironment, membrane organization and composition perturb nAChRs function. We postulate that nAChRs have a gain of function in disordered membrane environments but a loss of function in ordered ones, and that Chol molecules at the outer leaflet in annular sites and at the inner leaflet in non-annular sites are related to nAChR gating and desensitization, respectively. Thus, depending on the membrane composition, organization, and/or order, the nAChR adopts different conformations and locates in distinct lipid domains and this has a direct effect on its function.

1. Introduction

Nicotinic acetylcholine receptors (nAChRs) are integral membrane pentameric proteins that belong to the Cys-loop superfamily of ligand-gated ion channels [1–4]. Each of the 5 subunits contain a large extracellular domain, which carries the agonist-binding site, a transmembrane region which exhibits extensive contacts with the surrounding lipids through structural motifs conserved along phylogenic evolution [5–9], and an intracellular region that contains sites for receptor modulation and determinants of channel conductance [10,11]. The transmembrane domain is composed of four segments (TM1-TM4). The TM2 segments form the ion channel pore [11,12] and TM1, TM3, and TM4 are located more externally. Among them, TM4 is the most peripheral segment and is in closest contact with the membrane lipids. This is the reason why it is considered a lipid sensing domain [13–15]. The binding to the nAChR of its natural agonist, acetylcholine (ACh), triggers a conformational change that results in the opening of the ion

---

Abbreviations

ACh	acetylcholine;
bSM	brain sphingomyelin
carb	carbamylcholine;
CHEMS	cholesteryl hemisuccinate
Chol	cholesterol
ChOx	cholesterol oxidase
CrV	Crystal violet;
DiI-C18	1,1′-dioctadecyl-3,3,3′,3′-tetramethylindocarbocyanine perchlorate
DOPC	1,2-Dioleoyl-*sn*-glycero-3-phosphocholine;
DPH	1,6-Diphenyl-1,3,5-hexatriene
ECS	extracellular solution
eSM	egg sphingomyelin

FRAP	Fluorescence Recovery After Photobleaching
GP	Generalized Polarization
GUVs	Giant Unilamellar Vesicles
K_D	CrV dissociation constant
Ld	liquid-disordered domains
Lo	liquid-ordered domains
LUVs	Large Unilamellar Vesicles
nAChR	Nicotinic acetylcholine receptor
POPC	1-Palmitoyl-2-oleoyl-*sn*-glycero-3-phosphocholine;
P_{open}	open probability of the nAChR
TLC	Thin layer chromatography
TMA-DPH	1-(4-trimethylammoniumphenyl)-6-phenyl-1,3,5-hexatriene
TNBS	2,4,6-Trinitrobenzenesulfonic acid

channel and a flux of positive ions across the membrane, causing membrane depolarization and a subsequent intracellular cascade of events [10,16–18].

In vertebrates, seventeen different nAChR subunits can combine to yield a variety of receptors with different pharmacology, function, and location [19]. The most studied nicotinic acetylcholine receptor is the muscle nAChR, which is the paradigm of not only all other nAChRs but also of the entire Cys-loop superfamily. Either embryonic or adult-type muscle nAChRs are heteromeric receptors composed of α1$_2$, β1, δ, and ε/γ. These receptors are in high-density clusters in the neuromuscular junction where they participate in muscle contraction [20].

The nAChR is a transmembrane protein. Both the properties and the characteristics of the membrane where it is embedded are essential for its function as well as for its biosynthesis and correct assembly [21–25]. At the same time, the nAChR influences its nearby lipids [6,25–31]. A layer of immobilized lipids with different characteristics from those of bulk lipids encircles the muscle nAChR [26] where two different populations of lipids, namely non-annular and annular lipids [27], can be distinguished. Non-annular lipids are in close contact with the protein, probably in between the transmembrane segments associated to lipid binding sites and have a slow exchange rate with bulk lipids. In contrast, annular lipids interact with the protein in a relatively less specific manner and have a fast rate of exchange with bulk lipids [33–36]. Furthermore, given that lipids change with aging and in response to different neurodegenerative diseases [37,38] and that they also vary in different tissues, it is crucial to understand how changes in the nAChR lipid environment produce an impact on its structure and activity.

Due to the abundance of Chol in cell membranes and its importance and implication in different human diseases, a great deal of research has focused on the influence of this lipid on nAChR function. As an annular lipid, and in the rest of the membrane, Chol plays an important role conditioning the physical properties of the environment probably because of its participation in Chol-rich domains formation and in the maintenance of the asymmetrical membrane condition. As a non-annular lipid, the occurrence of allosteric binding sites has been demonstrated [27,29,39]. Identification of 15 cholesterol molecules at association sites in the nAChR was first reported by Marsh et al. [26]. Later, using molecular dynamics simulations of the nAChR structure, Branningan et al. [41] identified 15 Chol binding sites in large hydrophobic inter- and intrasubunit gaps. The location of Chol molecules at the intersubunit sites improves nAChR stability and the occupation of intrasubunit sites by Chol precludes the nAChR from collapsing [40,41]. More recently, by crioelectromicroscopy of *Torpedo* membranes, two regions for Chol at the receptor-lipid interface were distinguished: a low-affinity one in the outer hemilayer in between three TM domains (TM1, TM3, and TM4) and a high affinity one in the inner hemilayer in relation to TM4, TM1, and Mx [13,42]. In addition to this,

bioinformatics studies revealed the existence of CRAC motifs (Cholesterol Recognition Amino acid Consensus) and one CARC (inverted CRAC) motif [43,44] in nAChRs, which could facilitate the interaction between nAChRs and Chol.

In the present work, we focused on the possibility of a two-way physiological relationship between the nAChR and its surrounding membrane. To this end, we carried out different biophysical studies exploiting the advantages of several model systems in an attempt to understand the importance of the membrane environment in nAChR function and vice versa. Each model system was either treated with more Chol or with cholesteryl hemisuccinate (CHEMS), which has a succinate acid with a net negative charge at pH 7.4 preventing it from flip-flopping across the membrane [45], or was incubated with the enzyme cholesterol oxidase (ChOx) that oxidizes Chol molecules to cholestenone [46–48]. Model systems were also prepared in either the absence or presence of a peptide corresponding to the TM4 segment of the γ subunit of the nAChR (γTM4). Thin layer chromatography (TLC) of lipid extracts confirmed membrane sterol modifications, and studies of membrane order using the fluorescent probes 1,6-diphenyl-1,3,5-hexatriene (DPH), 1-(4-trimethylammoniumphenyl)-6-phenyl-1,3,5-hexatriene (TMA-DPH) and Laurdan provided information about subsequent membrane order perturbations. Fluorescence studies with Crystal violet (CrV) and electrophysiological studies both at the cell-attached and whole-cell patch-clamp configurations allowed us to correlate Chol changes with nAChR conformation and function, respectively. Furthermore, fluorescence microscopy of cell-sized giant unilamellar vesicles (GUVs) was used to analyze the effect of each treatment on lipid ordered domains, on lipid-nAChR interaction, and on nAChR location. This information allowed us to correlate the effects caused by Chol modifications with nAChR function. Our results show a feedback relationship between membrane organization and nAChR function. We postulate that nAChRs present a gain of function in disordered membrane environments but a loss of function in ordered ones. Furthermore, Chol molecules at the outer leaflet in annular sites and at the inner leaflet in non-annular sites are related to nAChR gating and desensitization, respectively.

2. Materials and methods

2.1. Materials

Torpedo californica specimens obtained from the Pacific coast of California (Aquatic Research Consultants, San Pedro, CA, USA) were killed by pithing, and the electric organs were dissected and stored at −70 °C until use. A 28-mer synthetic peptide representing the *T. californica* nAChR γM4 transmembrane segment and its two extra-membranous regions (sequence DKACFWIALLLFSIGTLAIFLTGHFNQV;

> 90% pure) was purchased from Biosynthesis, Inc. (Lewisville, TX) and kepted lyophilized at −80 °C until use. Cholesterol (Chol), brain sphingomyelin (bSM), egg sphingomyelin (eSM), 1,2-Dioleoyl-*sn*-glycero-3-phosphocholine (DOPC) and 1-Palmitoyl-2-oleoyl-*sn*-glycero-3-phosphocholine (POPC) were from Avanti Polar Lipids, Inc. 1,1′-dioctadecyl-3,3,3′,3′-tetramethylindocarbocyanine perchlorate (DiI-C18) was purchased to Invitrogen. Acetylcholinesterase (type VIS lyophilized powder), crystal violet (CrV), alpha-bungarotoxin (α-BTX), Cholesteryl hemisuccinate (CHEMS), cholesterol oxidase (ChOx) from *Streptomyces* sp., 7-Diethylamino-3-(4′-Maleimidylphenyl)-4-Methylcoumarin and all the other drugs used in the present study were obtained from Sigma-Aldrich.

2.2. Methods

2.2.1. nAChR-rich membrane preparation

Crude nAChR-membranes were prepared from the electric organ of *T. californica* as previously described [49]. The electric tissue was first chopped into small pieces, and then homogenized at 4 °C using a Virtis 60 glass (The Virtis Co., Inc.) until a homogeneous suspension was obtained. The homogenate was subjected to a first centrifugation at 2500 g at 4 °C for 10 min, and the obtained supernatant was subsequently centrifuged at 30,000 g at 4 °C for 1 h. Crude membranes were obtained by resuspending the pellet. nAChR-rich membranes were obtained by centrifuging the crude membrane fractions on a sucrose gradient (50%, 39% and 35% sucrose) at 30,000 g at 4 °C for 1 h [49]. The middle fraction corresponds to nAChR-rich membranes with a specific activity of 1.0–1.5 nmol of α-BTX sites/mg of protein [49].

2.2.2. LUVs preparation

Aliquots of POPC, bSM, and Chol dissolved in chloroform:methanol (2:1 v/v) were mixed to obtain the lipid composition POPC:SM:Chol (1:1:1 M ratio). The samples were first dried under nitrogen for 1 h and then Dialysis Buffer (100 mM NaCl, 0.1 mM EDTA, 0.02% NaN$_3$, 10 mM phosphate, pH 7.4) was added (final concentration 0.5 mg/ml), thus obtaining multilamellar vesicles. Large unilamellar vesicles (LUVs) were obtained by extrusion of multilamellar vesicles suspensions using a syringe LiposoFast-Basic (Avestin Inc., Canada) and membrane filters with a pore size of 100 nm.

2.2.3. GUVs electroformation

Two main compositions were explored: one with eSM and one with bSM, as set by availability in the labs. When working with eSM, 10 μl of a 4 mM chloroform lipid solution composed of POPC:Chol:eSM (1:1:1) or DOPC:Chol:eSM (1:1:1) containing 0.1 mol % DiI-C18, with or without a synthetic peptide corresponding to the TM4 segment of the nAChR γ subunit (lipid to peptide molar ratios (L:P) 125:1 or 250:1) were spread on a pair of conductive glasses coated with indium tin oxide (ITO) and the latter were kept under vacuum at room temperature for 1 h to evaporate the organic solvent. The glasses were placed with their conductive sides facing each other, separated by a 2 mm thick Teflon spacer to form a chamber. The lipid films were hydrated with 100 mM sucrose solution. The conductive glasses were connected to a function generator and alternating current of 1.1 V and 10 Hz frequency was applied at 60 °C for 1 h. After electroformation, the vesicles were cooled down to room temperature (23 °C). The obtained GUVs were harvested and diluted with an isoosmolar glucose solution before observation under the microscope. Vesicles containing γTM4 peptide were incubated with a solution of coumarin in DMSO at room temperature for 2 h. The thiol-reactive coumarin is very weakly fluorescent until reacted with thiols, producing a conjugate with excitation/emission maxima of ~384/470 nm. The peptide:coumarin molar ratio was 1:10–1:20. GUVs were directly observed using a confocal microscope (Leica microsystems TCS SP5 or SP8, Wetzlar, DE) equipped with a 63 × /1.4 NA water immersion objective. DiI-C18 fluorescence was excited by using a 561 nm diode-pumped solid state laser with emission collected in the range

567–606 nm and coumarin by a 405 nm diode laser with emission collected in the range 415–480 nm.

When working with bSM, 10 μl of an 8 mM ethanol lipid solution of POPC:Chol:bSM (1:1:1) were spread on an ITO coated glass from the Vesicle PrepPro (Nanion, Munich, Germany). The glass was kept under nitrogen at room temperature for 1 h to evaporate the organic solvent, and 250 μl of a 450 mM sucrose solution were subsequently added to the obtained lipid film. The glass was placed with its conductive side facing another glass conductive side, separated by a ring spacer to form a chamber. GUVs were electroformed by applying an alternating current of 1.1 V and 10 Hz frequency at 60 °C for ~1.30 h. After electroformation, the vesicles were cooled down to room temperature. DiI-C18 was added either to the ethanol lipid solution at a 0.1 mol% or to the obtained GUVs from an ethanol solution (0.5% v/v). The obtained GUVs were diluted with a glucose isoosmolar solution and directly observed using a confocal Laser Scanning Microscope (Olympus, FV100 or Leica, TCS SP2) equipped with a 63x/1.4 NA water immersion objective. DiI-C18 was excited by using a 543 nm He–Ne laser with emission collected at 560–630 nm.

2.2.4. Membrane cholesterol modification

An aliquot of an ethanol solution of Chol or CHEMS was added to a suspension of LUVs, GUVs, or nAChR-rich membranes (final concentration <0.1% v/v organic solvent) and incubated at room temperature for 30 min. For the treatment with ChOx, model systems were incubated with the enzyme (5U enzyme/100 μl) at room temperature for at least 30 min. For all the experiments, control conditions were obtained with the addition of only ethanol.

2.2.5. Lipid analysis

Protein-free LUVs composed of POPC:Chol:bSM (1:1:1), exposed to the different treatments, were separated by centrifugation at 4500 rpm at 23 °C for 30 min using Amicon Ultra-0.5 centrifugal filter devices with a 100 kDa molecular weight cutoff in a microcentrifuge Eppendorf 5415C. After centrifugation, LUVs were retained above the membrane filter, and were collected for lipid analysis. Lipids from concentrated samples were extracted according to the procedure of Bligh and Dyer [50] and resolved into classes by TLC. Chloroform:methanol:ammonia (65:25:4, v/v/v) was run up to approximately the middle of the plates to separate PC from SM, and, after drying the plates, hexane/ether (60:40, v/v) was run up to the top of the plates to resolve sterols. For visualization and subsequent analysis, the plates were sprayed with an aqueous solution of 3% p/v cupric acetate 8% v/v phosphoric acid and heated. Lipid semi-quantification was performed using the ImageJ 1.43u program (NIH) and results were expressed as the Chol/bSM ratio.

2.2.6. Miscibility temperature

For miscibility temperature evaluation, epifluorescence microscopy (Axio Observer. D1, Zeiss, Oberkochen, Germany) was employed. DOPC: eSM:Chol (1:1:1) vesicles, with or without γTM4, were introduced into a custom-made chamber with temperature controlled by circulating water connected to a thermostat [51,52]. The initial temperature was set to 22 °C and it was then increased by 2 °C. GUVs were incubated for 10 min at each temperature before counting the number of phase-separated vesicles from a total of 100 vesicles with sizes larger than roughly 50 μm. The fraction of homogeneous vesicles at each temperature was plotted against temperature (°C) and fitted to a sigmoidal Boltzmann model, see Ref. [51] for further details. As the miscibility transition has a sigmoidal behavior, once the fraction value is measured to be 0 at a certain temperature all fraction values of the temperature range below are considered to be 0. Vice versa, once the fraction value is 1 at a particular temperature, all fraction values of the temperature range above are assumed to be 1.

2.2.7. Fluorescence recovery after photobleaching (FRAP)

FRAP measurements were performed on the liquid disordered do-

mains on GUVs composed of DOPC:Chol:eSM (1:1:1) for three cases: (i) GUVs without γTM4, (ii) GUVs with γTM4 (L:P 250:1), and (iii) GUVs with γTM4 (L:P 125:1). Images with size 256 x 256 pixels were recorded with a confocal microscope at 1000 Hz; the scanning mode was set to bidirectional. The pinhole size was set to 1 Airy unit. A HC PL APO CS2 63x/1.20 water objective was used. Measurements were performed at room temperature (23 °C). Dil-C18 was excited with the 561 nm laser line and the fluorescence signal collected at 567–606 nm. Ten frames at attenuated laser intensity (4.4%) were recorded before the bleaching. Photobleaching was performed for 3 frames (505 ms) at 100% laser intensity using a circular region of interest (ROI) of nominal radius $r_n = 2.5$ μm. The post-bleach recovery images were subsequently recorded at the initial attenuated laser intensity for 50 frames. The diffusion coefficient (D) was extracted using $D = (r_e^2 + r_n^2)/(8t_{1/2})$ were r_e and r_n are the effective and the nominal radii, respectively, and $t_{1/2}$ is the halftime for the photorecovery of the dye [53], see Ref. [54] for further details.

2.2.8. Fluorimetric measurements

Fluorimetric measurements were performed in a SLM model 4800 fluorimeter (SLM Instruments, Urbana, IL) using a vertically polarized light beam from Hannovia 200-W mercury/xenon arc obtained with a Glan-Thompson polarizer (4-nm excitation and emission slits).

2.2.8.1. - nAChR conformational state characterization. nAChR-rich membranes were resuspended in buffer A (150 mM NaCl, 0.25 mM MgCl₂, and 20 mM HEPES buffer, pH 7.4) at a final concentration of 100 μg of protein/ml. Fluorimetric measurements were performed in 2 ml quartz cuvettes. nAChR conformational changes were evaluated using Crystal violet (CrV) as described previously [32,55]. For the measurements conducted with the nAChR in the desensitized state, *T. californica* membranes were afterwards incubated with 1 mM of carbamylcholine (carb) for 15 min. The membranes were subsequently titrated with increasing concentrations of CrV (in buffer A). After each addition of CrV, the samples were incubated for 15 min before obtaining the fluorescence emission spectra. CrV was excited at 600 nm, and the fluorescence emission spectra were collected from 605 to 700 nm. Before the first addition of CrV, a background fluorescence emission spectrum was obtained for each sample. The spectrum was subsequently subtracted from the emission spectra obtained in the presence of CrV and the maximum intensity (at 623–625 nm) was measured. To determine the CrV dissociation constants (K_D), the values of CrV maximum fluorescence emission were plotted as a function of the logarithmic CrV concentrations (M). The resulting sigmoid curve was fitted to the Boltzmann function and K_D was calculated.

2.2.8.2. - Generalized polarization (GP). Excitation GP (exGP) was calculated as follows [56]:

$$GP = (I_{434} - I_{490}) / (I_{434} + I_{490})$$

Where I_{434} and I_{490} are the emission intensities at the characteristic wavelength of the gel phase (434 nm) and the liquid crystalline phase (490 nm), respectively. Excitation GP values were obtained from emission spectra of Laurdan obtained with an excitation wavelength of 360 nm.

2.2.8.3. - Fluorescence anisotropy. Anisotropy (r) measurements of DPH or TMA-DPH (0.6 mM final concentration) were made as described previously [28,57]. The excitation and emission wavelengths used were 365 and 425 nm, respectively. Fluorescence anisotropy measurements were performed in the T format with Schott KV418 filters in the emission channels and corrected for optical inaccuracies and background signals. The anisotropy value, r, was obtained according to the following equation [58]:

$$r = [\ (I_v/I_h)_v - (I_v/I_h)_h \ ] \ / \ [\ (I_v/I_h)_v + (I_v/I_h)_h \ ]$$

Where $(I_v/I_h)_v$ and $(I_v/I_h)_h$ are the ratios of the emitted vertically or horizontally polarized light to the excited vertically or horizontally polarized light, respectively.

2.2.8.4. - Quenching of TMA-DPH or DPH emission by 2,4,6-Trinitrobenzenesulfonic acid (TNBS). DPH or TMA-DPH labeled LUVs (final cuvette volume: 2 ml) were titrated with increasing amounts of TNBS from a stock solution of 200 mM TNBS in buffer A at room temperature (cuvette TNBS concentrations were 0.25, 0.5, 1, 1.5, 2, and 4 mM). After each addition, the samples were incubated for 30 min before fluorescence anisotropy measurements.

2.2.9. Cell culture and transfection

Each nAChR cDNA subunit was sub-cloned into the pRBG4 plasmid for heterologous expression. HEK293 cells were transfected with mouse α1, β1, δ, and ε subunits in a ratio 2:1:1:1 (for adult muscle nAChR, α1₂β1δε) using calcium phosphate precipitation as was previously described [59,60]. For electrophysiological measurements, a plasmid encoding green fluorescent protein (GFP) was included in all transfections to allow the identification of transfected cells under fluorescence optics.

2.2.10. Electrophysiological experiments

HEK293 cells expressing muscle nAChR were used for single-channel and macroscopic currents measurements two or three days after transfection.

Single-channel recordings were performed in the cell-attached patch-clamp configuration at room temperature (23 °C) and at −70 mV of membrane potential. The bath and pipet solutions contained 142 mM KCl, 5.4 mM NaCl, 1.8 mM CaCl₂, 1.7 mM MgCl₂, and 10 mM HEPES, and pH 7.4. ACh was added to the pipette solution up to 30 μM as a final concentration. Single-channel currents were recorded using an Axopatch 200 B patch-clamp amplifier (Molecular Devices), digitized at 200 kHz, and low-pass filtered at a cutoff frequency of 10 kHz using an Instrutech ITC-18 (HEKA Instruments Inc.) computer interface. Single-channel events were idealized by the half amplitude threshold criterion using the QuB 2.0.0.28 program (www.qub.buffalo.edu) with a digital low-pass filter at 9 kHz. The open and closed time durations were estimated from the idealized recordings by the maximum interval likelihood (MIL) function in QuB with a dead time of 0.03 ms, which is the interval duration below which events cannot be resolved [61,62]. Therefore, only transitions longer than the dead time were accepted and used to construct the duration histograms. This analysis was performed on the basis of a kinetic model whose probability density function curves properly describe the histograms following the maximum likelihood criteria. The best description was obtained with the classical kinetic model previously reported for this receptor [59,60]. Clusters were identified as a series of closely separated openings originated from the same receptor molecule preceded and followed by closings longer than a critical duration. Different critical closed times were calculated by MIL between each closed component. Critical time between the second and third closed components for the muscle nAChR (~15 ms) was selected in QuB to chop the idealized data and create a sub-data set that only contained clusters to define mean cluster duration and open probability within clusters (P_open).

To evaluate nAChR modulation, the culture media was replaced by 2 ml of the experimental drug solution (containing CHEMS or ChOx) prepared in the same culture media at the corresponding final concentration. After incubation, the media was replaced by 1 ml of bath solution and cells were used to obtain the corresponding single-channel recordings.

Macroscopic currents were obtained in the whole-cell configuration. The pipette solution contained 134 mM KCl, 10 mM HEPES, 5 mM EGTA and 1 mM MgCl2, and pH 7.4. The extracellular solution contained 150 mM NaCl, 10 mM HEPES, 1.8 mM CaCl₂ and 1.0 mM MgCl₂, and pH 7.4.

To evaluate nAChR modulation by ChOx, macroscopic currents were obtained from transfected cells before (control) or after (experimental) incubation at two different times (90 and 230 min). For these experiments, the perfusion system consisted of solution reservoirs, manual switching valves, a four-channel valve controller (ALA Scientific System), a solenoid-driven pinch valve, and three silicon tubes (inner diameter 0.3 mm, from Cole-Parmer) inserted into the culture dish and oriented towards the cell [63,64]. Initially, the cell was continuously perfused with extracellular solution (ECS) from one tube to maintain the receptors in the resting state. To obtain control responses, 1-s pulses of 300 μM ACh prepared in ECS were applied from the second tube. After obtaining the control currents, a 30 to 60-s pulse of CHEMS prepared in ECS at different concentrations was applied to the same cell followed by a new pulse of ACh to obtain the modulated current. The stability of the seal and the absence of rundown were confirmed by a new control pulse of ACh alone after 30-s washout. Macroscopic currents were recorded with the already mentioned equipment for the single-channel recordings, at -50 mV membrane potential, and were filtered at 5 kHz and digitalized at 20 kHz. Currents were acquired with WinWCP 5.3.2 (University of Strathclyde, Glasgow, Scotland) and analyzed using Clampfit 10.7.0.3 (Molecular Devices, San José, CA). Each current represents the average from more than 3 individual traces obtained from the same seal. From macroscopic currents we analyzed the peak current, the rising time, which is the time (ms) that takes the response to rise from 10 to 90% ($t_{10-90\%}$) of the total response, and the decay time, which is obtained by fitting currents with the single exponential function:

$$I_{(t)} = I_0 \exp(-t/\tau_d) + I\infty$$

Where I_0 and $I\infty$ are the peak and steady state values (in pA), respectively, and τ_d is the decay time constant (in ms).

To evaluate the recovery from desensitization, a 300-ms pulse of 300 μM ACh was applied to allow both activation and full desensitization of the receptors in the cell. After agonist washout, a second pulse of 300 μM ACh was applied at different delays from 100 to 1000 ms (interpulse time). The fractional recovery of the current elicited by the second pulse was plotted against the interpulse time. The curve obtained was fitted by the equation:

$$I_r(t) = 1 - \exp(-t/\tau_r)^n$$

Where I_r is the relative peak current and τ_r is the recovery time constant.

2.3. Data analysis

In the electrophysiological experiments a comparison of two mean values was performed through Student's t-test whereas in the fluorescence experiments a comparison of more than two mean values was made by analysis of variance (ANOVA), followed by post hoc test analysis of multiple comparisons Bonferroni. Differences were considered significant at $p < 0.05$ and highly significant at $p < 0.01$. In the case of n = 3, the data were considered if the coefficient of variation (standard deviation/media) was <0.1. Comparison between two data lines was performed by ANCOVA (covariance analysis) test after it was ensured that the variance in the two groups of data was the same. The null hypothesis states that for two data lines to be the same, their slopes must be equal. The null hypothesis was rejected with a p value < 0.05.

3. Results

To study the importance of Chol for nAChR location and function, we worked with different model systems which were exposed to various treatments in order to modify their initial Chol amount and/or location in the membrane.

LUVs composed of POPC:Chol:bSM (1:1:1) were initially used to verify that each treatment caused the expected sterol perturbation. With this lipid composition, the inner and outer leaflet of the membranes are symmetrical and there is a coexistence of liquid-ordered (Lo) and liquid-disordered (Ld) nanoscopic domains [65]. First, TLC was used to resolve the lipids (Figure S1 A) and a semi-quantitative analysis of each spot was performed using Image J 1.43u (NIH, USA) to evaluate the amount of Chol after the treatments (Figure S1 B). Total Chol increased by ~50% relative to bSM when LUVs were incubated in a buffer containing Chol added from an ethanol solution. Incubation of LUVs in a buffer containing CHEMS added from an ethanol solution resulted in an increase in the sterol:SM ratio from 1.0 to 1.7 and a total lipid molar ratio change from 1/3 (33%) to 1.7/3.7 (46%). The incubation of LUVs with ChOx led to a reduction in the sterol:SM ratio from 1.0 to 0.8 and cholestenone was observed as a new spot in the TLC, corroborating the oxidation of Chol due to the enzymatic activity.

To verify if each treatment caused changes in membrane order, we worked with LUVs composed of POPC:Chol:bSM (1:1:1) and nAChR-rich membranes from *T. californica* and performed membrane anisotropy measurements with the fluorescent probes DPH and TMA-DPH, and GP analysis using the fluorescent probe Laurdan. DPH is located at the hydrophobic core of the membrane, whereas TMA-DPH, a cationic derivative of DPH that remains anchored at the polar head group region, is located mainly in the outer leaflet [66,67]. Laurdan resides in both lipid leaflets at the polar head group region [28]. An increment of membrane anisotropy and GP values can be correlated with an increase in membrane order, while a decrease of those values is associated with a more disordered environment [29,68–70]. In this way, and to interpret them together, membrane order values were overall discussed. Similar effects were observed with both model systems (Table S1) even though in all cases higher values were observed with nAChR-rich membranes due to their more complex composition.

The lipid order of both nAChR-rich membranes and LUVs with increased Chol content (n = 3) was similar to that under the control condition (n = 3). Thus, although there was an effective incorporation of Chol, the increment in this lipid did not lead to a greater membrane order. Soto-Arriaza et al. [71] reported that the effect of Chol on membrane properties of binary and ternary model systems displays a maximum at 33.3 mol%, which, in our experiments, corresponds to the percentage of the control condition. When model systems were treated with ChOx (n = 3), the resulting membrane order was also like that under the control condition. The enzymatic treatment did not change the total amount of sterol molecules, and evidently the chemical modification of Chol molecules did not affect the membrane order.

A different result was obtained when both model systems were enriched in CHEMS (n = 3). Unlike the behavior observed with Chol, under this condition the membrane order was significantly increased. In a previous study we also observed a slight GP increment in *T. californica* nAChR-rich membranes after the addition of small quantities of CHEMS [72]. Although both molecules partition in the membrane with a similar effect [45], here we could differentiate an increment in either Chol or CHEMS. The main difference between them is that CHEMS has a succinate acid with a net negative charge at pH 7.4 which positions the molecule closer to the membrane-water interface [45] and prevents it from flip-flopping across the membrane. Thus, the measured increment probably corresponds to perturbations of the outer leaflet. To verify this, additional experiments were carried out. We measured DPH and TMA-DPH fluorescence anisotropy in the presence of either Chol or CHEMS and the polar-quenching molecule TNBS, which can only access to the fluorescent molecules located at the outer leaflet. Fig. S2 shows that under all conditions (both in the absence and presence of Chol or CHEMS) there was an increment in DPH and TMA-DPH anisotropy values as a function of TNBS concentration (Fig. S2). The slopes of the curves obtained after incubation with DPH and TMA-DPH were similar under the control condition (confirmed by ANCOVA, Figure S2 A) as well as under the condition with increased Chol content (confirmed by ANCOVA, Figure S2 B) although in the latter case, the values were higher. The similarity of the slopes observed with DPH and TMA-DPH under both conditions (control situation and with addition of Chol)

suggests that the bilayer is symmetric. In contrast, after addition of CHEMS, the slopes of the curves obtained with DPH and TMA-DPH were different (confirmed by ANCOVA, Fig. S2 C). The slope of the curve after incubation with TMA-DPH was similar to the one obtained under the condition with excess of Chol (confirmed by ANCOVA), whereas the slope for DPH was similar to that obtained under the control condition (confirmed by ANCOVA). The difference observed supports the idea of a difference between inner and outer leaflets, the inner leaflet being similar to that of the control condition and confirming that CHEMS is located mainly in the outer leaflet.

3.1. Implication of membrane Chol in nAChR function

To explore how variations in Chol content affect nAChR function, we first studied the receptor conformational state under each experimental condition. The nAChR can adopt three different and interconvertible major conformational states, namely resting state (R), in the absence of agonist, open state (O), and desensitized state (D), in the continuous presence of agonist. To study the conformational state of the nAChR, we used the nAChR conformational-sensitive fluorescence probe CrV [32, 55,57], which displays a higher affinity for the D than for the R state [73]. The value of the K_D of the CrV was used to infer the conformational state of the receptor [32,55]. To this end, *T. californica* nAChR-rich membranes were incubated either with Chol, CHEMS or ChOx in the absence and presence of carb, a full agonist for nAChRs.

When membranes were incubated with Chol (n = 4), no change was observed with respect to the control condition (n = 5) neither with nor without carb (Fig. 1). This result is consistent with the fact that addition of more Chol did not change the membrane order. On the contrary, after incubation with CHEMS (n = 4), a difference with respect to control was observed. Although in the absence of carb K_D values were close to those obtained for the control condition (Fig. 1A), in the presence of carb, K_D values increased and were similar to the values obtained for the nAChR in a resting state (without carb, Fig. 1B). Thus, the increment of total sterols with CHEMS in the outer leaflet of the membrane altered the nAChR conformational state as well as the membrane order. However, at this point it was not possible to determine between the receptor effectively staying in a resting state (i.e., it stabilizes in a closed non-conducting state) or other possibilities, such as changing its velocity or time of desensitization.

When membranes were incubated with ChOx (n = 5), the K_D values obtained were similar in the absence and presence of carb, as well as under the control condition in a resting state (without carb) (Fig. 1). Thus, as it was observed in the presence of CHEMS, at this point it was not possible to resolve whether the oxidation of Chol molecules either

retains the nAChR in a resting situation or modifies its desensitization rate. Unlike in the presence of CHEMS, oxidation of Chol did not alter the overall membrane order.

To understand the molecular mechanism underlying the occurrence or non-occurrence of nAChR conformational changes, we used the patch-clamp technique to obtain single-channel events and macroscopic currents from HEK293 cells expressing the mouse muscle nAChR.

At 30 μM ACh, single-channel recordings (n = 9) showed events of 5.2 ± 0.6 pA. Events mainly appeared in groups -called clusters- of 120 ± 65 ms with a P_{open} of 0.4 ± 0.1 (Fig. 2). At this ACh concentration, open-time histograms were properly described by two exponential components, whose durations (and relative areas) were 1.39 ± 0.17 ms (0.66 ± 0.21) and 0.32 ± 0.18 ms (0.34 ± 0.18), similar to those previously reported [60,74]. Closed-time histograms were described by three or four components, in which the two briefest correspond to closings within clusters, whose mean durations (and relative areas) were 0.135 ± 0.090 ms (0.17 ± 0.07) and 1.518 ± 0.304 ms (0.74 ± 0.12), which were similar to those previously described for this receptor [60, 74].

To evaluate nAChR activity in the presence of CHEMS, cells expressing the muscle receptor were incubated with 170 μM CHEMS for 90 min. After incubation, single-channel recordings were obtained at 30 μM ACh (n = 9). Under this condition, single-channel events appeared mainly grouped in clusters with reduced duration (62 ± 27 ms, p = 0.02) and P_{open} (0.35 ± 0.06, p = 0.002) (Fig. 2). A clear reduction in open duration was observed since the open-time histograms were described mainly by a single exponential component whose mean duration was 0.75 ± 0.15 ms (p = 8.1 × 10^{-7}, Fig. 2). Closed-time histograms were described by four or five exponential components. The mean duration of closings within clusters were 0.26 ± 0.01 and 1.08 ± 0.33 ms, but a new component was observed (0.04 ± 0.01), which may indicate a new non-conducting state stabilized by the presence of CHEMS in the membrane.

These results demonstrate a negative modulation of the nAChR in the presence of CHEMS (briefer openings grouped into clusters with reduced duration and P_{open} than those observed under the control condition).

In order to evaluate nAChR function when part of the total amount of Chol was converted into cholestenone, the cells were incubated for 90 min with a solution containing 5U ChOx/100 μl DMEM. After incubation, the culture media was replaced by a bath solution and single-channel events elicited by 30 μM ACh were recorded. nAChR activation was similar to that under the control condition: single-channel events were grouped into clusters of 123 ± 37 ms (p = 0.49) with 0.4 ± 0.09 of P_{open} (p = 0.061). Cluster analysis showed that open- and closed-time histograms were described by the same number of
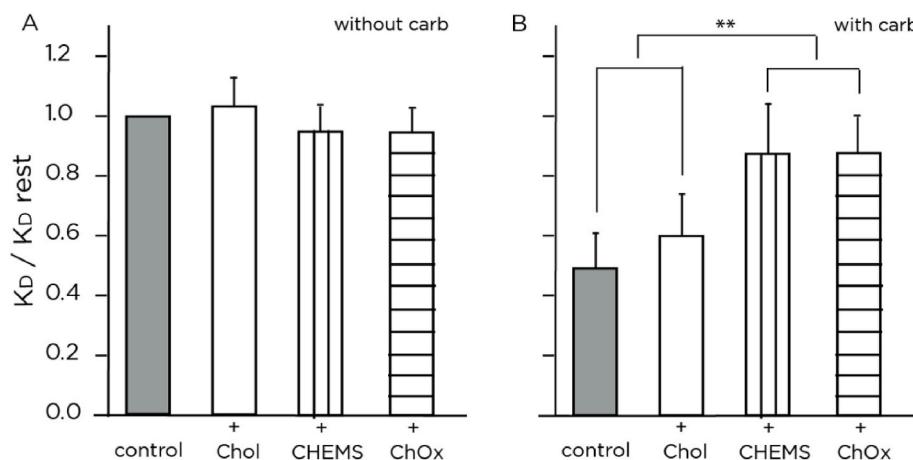

Fig. 1. Variations in the K_D-ratio of CrV expressed as the ratio between A) K_D values in the absence of carb and the control K_D obtained in the resting state, and B) K_D values in the presence of carb and the control K_D obtained in the resting state. Each column represents the average ± SD of the total number of samples of each condition. ** denote highly significant differences (p < 0.01).
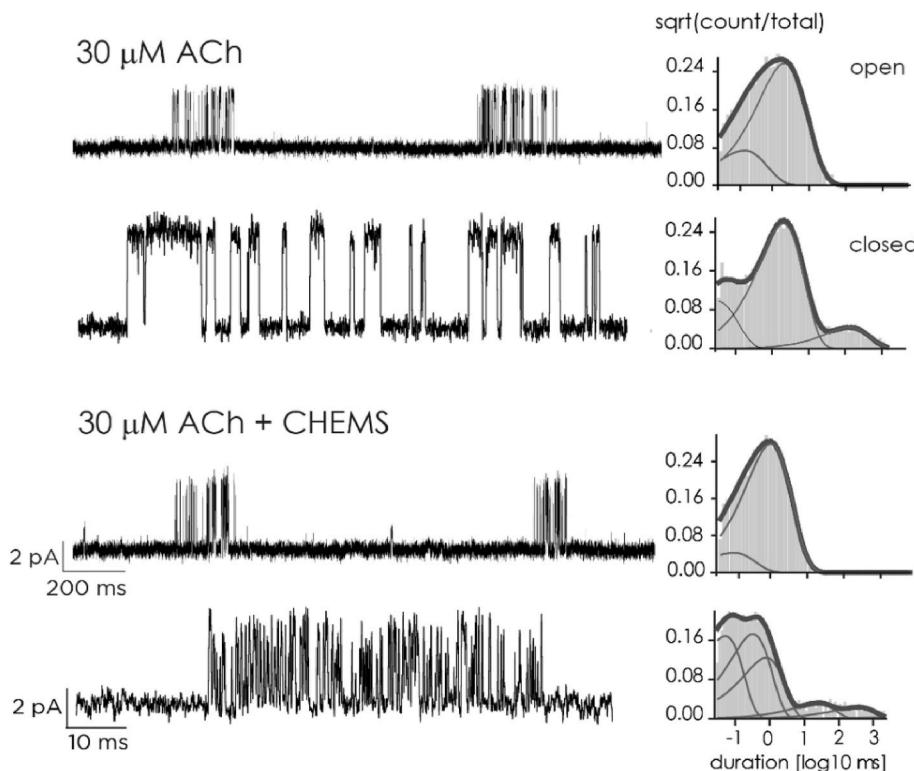
Fig. 2. nAChR modulation by the presence of CHEMS in the membrane. Single channel events obtained at 30 μM ACh before and after incubation of the cells with 170 μM of CHEMS. For each condition, one cluster is shown at two different temporal scales. Openings are shown as upward deflections separated by brief closings. Their corresponding open and closed duration histograms are shown on the right. Events were recorded in the cell-attached configuration at −70 mV of membrane potential.

exponential components as the control condition, with mean values of 1.35 ± 0.27 ms and 0.15 ± 0.09 ms for open durations, and 0.11 ± 0.02 and 1.69 ± 0.58 ms for closed durations within clusters.

Taking into account that CrV experiments showed changes in the nAChR conformational state after incubation with ChOx, contrary to what was observed in single-channel recordings, we performed patch-clamp experiments in the whole-cell configuration to obtain macroscopic currents. After rapid application of a 300 ms pulse of 300 μM ACh, a fast activated current was observed, whose rise time (obtained from the $t_{10–90\%}$ calculation) was 10 ± 4 ms and the decay time constant (fitted by a single-exponential component) was 115 ± 22 (n = 5) (Fig. 3 A), in coincidence with what was previously reported [75]. When currents were obtained from cells that were previously incubated with

ChOx for 90 min (n = 4) or 230 min (n = 4), we observed similar kinetic parameters to those recorded under control conditions. Their $t_{10–90\%}$ were 8 ± 4 ms and 7 ± 2 ms (with p = 0.588 and p = 205 with respect to control), and decay times were 190 ± 90 ms and 105 ± 20 ms (with p = 0.154 and p = 0.386 with respect to control) for 90 and 230 min, respectively.

To deepen the understanding of the mechanism through which ChOx provokes changes in nAChR activation, we measured recovery time after desensitization for cells under the control condition and after incubation with ChOx for 90 and 230 min. Our results showed that the time of recovery from desensitization was briefer in cells treated with ChOx than under the control condition (Fig. 3 A and B). The recovery time was 404 ± 78 ms (n = 4) for the control condition and 259 ± 59 ms (n = 4, p
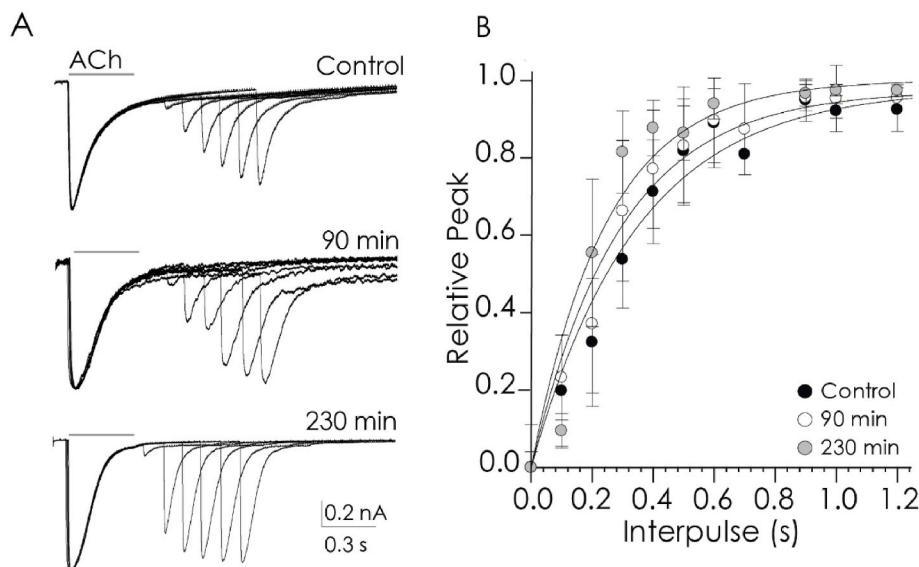

Fig. 3. Recovery from desensitization after incubation of cells with ChOx. A) nAChR macroscopic currents obtained in the whole-cell configuration before (control) and after incubation with ChOx at two different times (90 and 230 min). Test currents were recorded by applying a pulse of 300 μM ACh during 300 ms and a second pulse of ACh was perfused at different interpulse times. B) Relationship between the second and first pulse (Relative peak) plotted against the interpulse time and fitted by a single exponential function to obtain the recovery time for each condition (τ_r). τ_r values were 404 ± 78 ms, 259 ± 59 ms and 235 ± 66 ms for control, 90 and 230 min, respectively.

$= 0.029$ with respect to control) and 235 ± 66 ms (n = 4, p = 0.020 with respect to control) for the cells incubated with ChOx during 90 and 230 min, respectively.

Our results therefore showed that the oxidation of Chol into cholestenone modulates the nAChR by reducing the time needed to recover from desensitization without affecting other kinetic parameters. These results are in line with the fluorescence CrV results shown above, which indicated a perturbation of the nAChR conformation but could not provide any information about the desensitized state of the receptor.

3.2. Cholesterol changes and Lo domains

To further explore the effect of the different treatments on membrane organization and protein location, we performed experiments with GUVs, cell-sized vesicles in which the membrane response and behavior can be directly observed under the microscope [76,77]. GUVs were prepared with the same lipid mixture as the one used for LUVs (POPC: Chol:bSM, 1:1:1), a composition at which Lo-Ld phase coexistence is expected at 23 °C. However, the domains are transient and nanoscopic and cannot be observed under the microscope [65] unless there is an increment in Lo domains size, as previously demonstrated [78].

POPC:Chol:bSM (1:1:1) GUVs were labeled with DiI-C18, a fluorescent dye that is excluded from Lo domains. Vesicles were first incubated with Chol or CHEMS in order to evaluate whether there is a change in membrane organization under these conditions, but no differences were observed. Thus, neither symmetric incorporation of Chol (due to the flip-flop capacity of this molecule, Fig. 4 B) nor asymmetric incorporation of CHEMS (Fig. 4 D) resulted in a microscopic change of the Lo-Ld phase coexistence. We also prepared symmetric GUVs with compositions POPC:Chol:bSM (1:2:1) and POPC:Chol:CHEMS:bSM (1:1:1:1). In both cases, the vesicles were bigger than those described above (Fig. 4C and E, and Fig. S3). The majority of POPC:Chol:bSM (1:2:1) vesicles (~70–80%), unlike what was observed after incubation of POPC:Chol:

bSM (1:1:1) vesicles with Chol, exhibited several small microscopic domains. The difference observed between membranes with increased Chol fraction in the initial lipid ratio and membranes subjected to subsequent addition of this sterol suggests that only Chol fraction increment along the first path is sufficient to result in coalescence of domains to sizes detectable under the microscope. In contrast, no domains were observed in POPC:Chol:CHEMS:bSM (1:1:1:1) GUVs.

POPC:Chol:bSM (1:1:1) GUVs were also incubated with ChOx. After enzymatic treatment, in almost all cases (~80%) large microscopic Lo domains, covering ~40–50% of the vesicle area, could be observed (Fig. 4 F). The oxidation of ~25% of Chol possibly led to changes in membrane order and composition, with a displacement of cholestenone molecules from Lo domains [79–82], which could generate an exchange with Chol molecules initially located in Ld domains. Thus, both Ld and Lo domains may change their composition and probably their biophysical properties, resulting in the coalescence of the nanoscopic Lo domains that remained after treatment with ChOx.

The fact that the microscopic Lo domains observed in POPC:Chol: bSM (1:2:1) vesicles were different from those in POPC:Chol:bSM (1:1:1) vesicles after the treatment with ChOx, can be explained considering that Chol favors the formation of Lo phase whereas cholestenone tends to form Ld domains.

3.3. A model of how nAChRs condition their lipid microenvironment

We observed that changes in membrane composition have an impact on nAChR conformation and function. We next studied whether there is a two-way communication process, i.e. if the presence of the nAChR could alter the membrane environment organization and/or order. To deepen on this relationship, a peptide corresponding to the TM4 segment of the γ subunit of the nAChR (γTM4) was reconstituted in POPC:Chol:eSM (1:1:1) or DOPC:Chol:eSM (1:1:1) GUVs. Vesicles prepared from a lipid composition of DOPC:Chol:eSM (1:1:1), unlike those
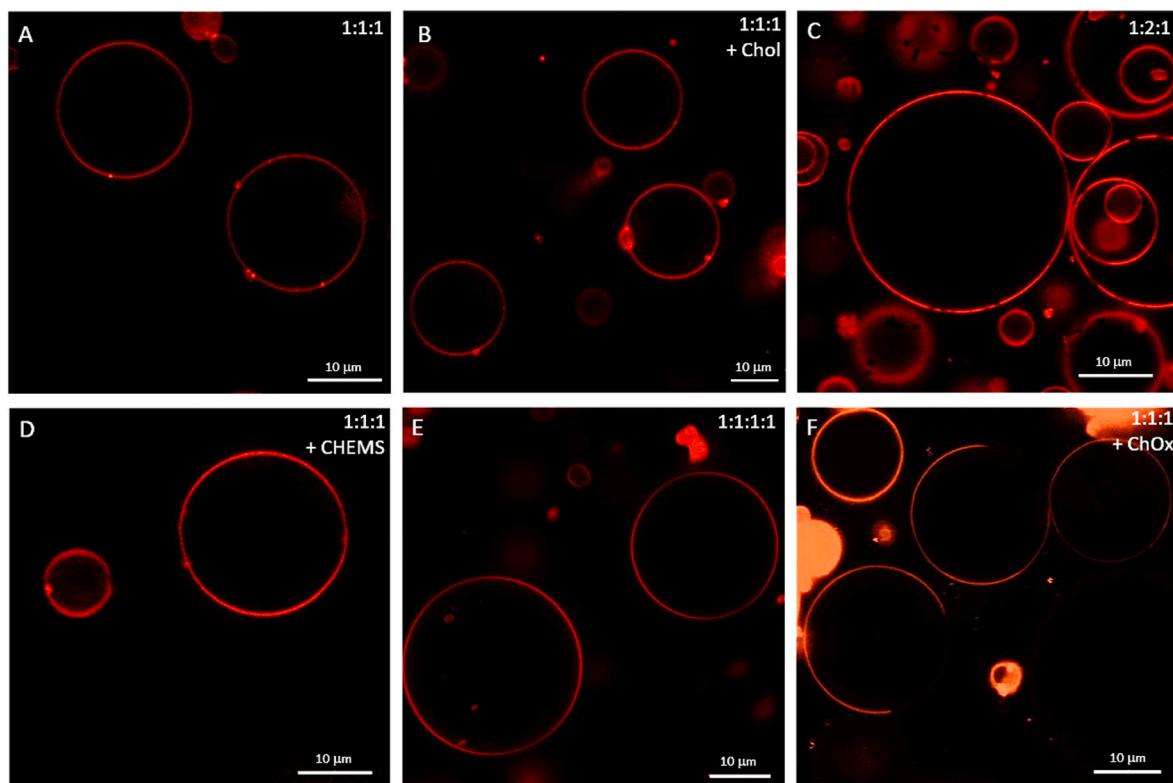

Fig. 4. Confocal microscopy of GUVs labeled with 0.1% DiI C-18. A) Vesicles composed of POPC:Chol:bSM (1:1:1) B) POPC:Chol:bSM (1:1:1) incubated with Chol; C) POPC:Chol:bSM (1:2:1); D) POPC:Chol:bSM (1:1:1) incubated with CHEMS; E) POPC:Chol:CHEMS:bSM (1:1:1:1); and F) POPC:Chol:bSM (1:1:1) incubated with ChOx.

made using POPC instead of DOPC, are phase-separated and exhibit coexistence of Lo and Ld micron-sized domains. Although DOPC is not typically found in cell membranes, it has been widely used in model membrane experiments to investigate phase separation in such ternary mixtures [83,84]. In both cases, control GUVs without the peptide were also prepared for comparison.

TM4 is the most external transmembrane segment of each subunit of the nAChR and hence in intimate contact with both the surrounding membrane lipids and the rest of the transmembrane segments, two facts that make this segment a key participant in the lipid-nAChR interaction [13–15].

Similarly to POPC:Chol:bSM (1:1:1), GUVs composed of POPC:Chol:

eSM (1:1:1) showed no phase separation (Fig. 5), which is in agreement with the fact that both bSM and eSM have similar SM/Chol interactions [85]. As it was expected, and in agreement with previous observations [84], in the majority of the vesicles prepared with DOPC:Chol:eSM (1:1:1) it was possible to observe phase separation with a roughly similar area fraction (~50%) of the Ld and Lo domains (Fig. 5 B).

DOPC:Chol:eSM (1:1:1) GUVs containing γTM4 in a 250:1 or 125:1 lipid:peptide (L:P) molar ratio appeared similar to those obtained in the absence of the peptide (Fig. 5). The vesicles showed similar size, shape, and coexistence of domains compared to the ones without the peptide. In the case of POPC:Chol:eSM (1:1:1) vesicles containing γTM4, different results were obtained depending on whether the L:P ratio was 250:1 or
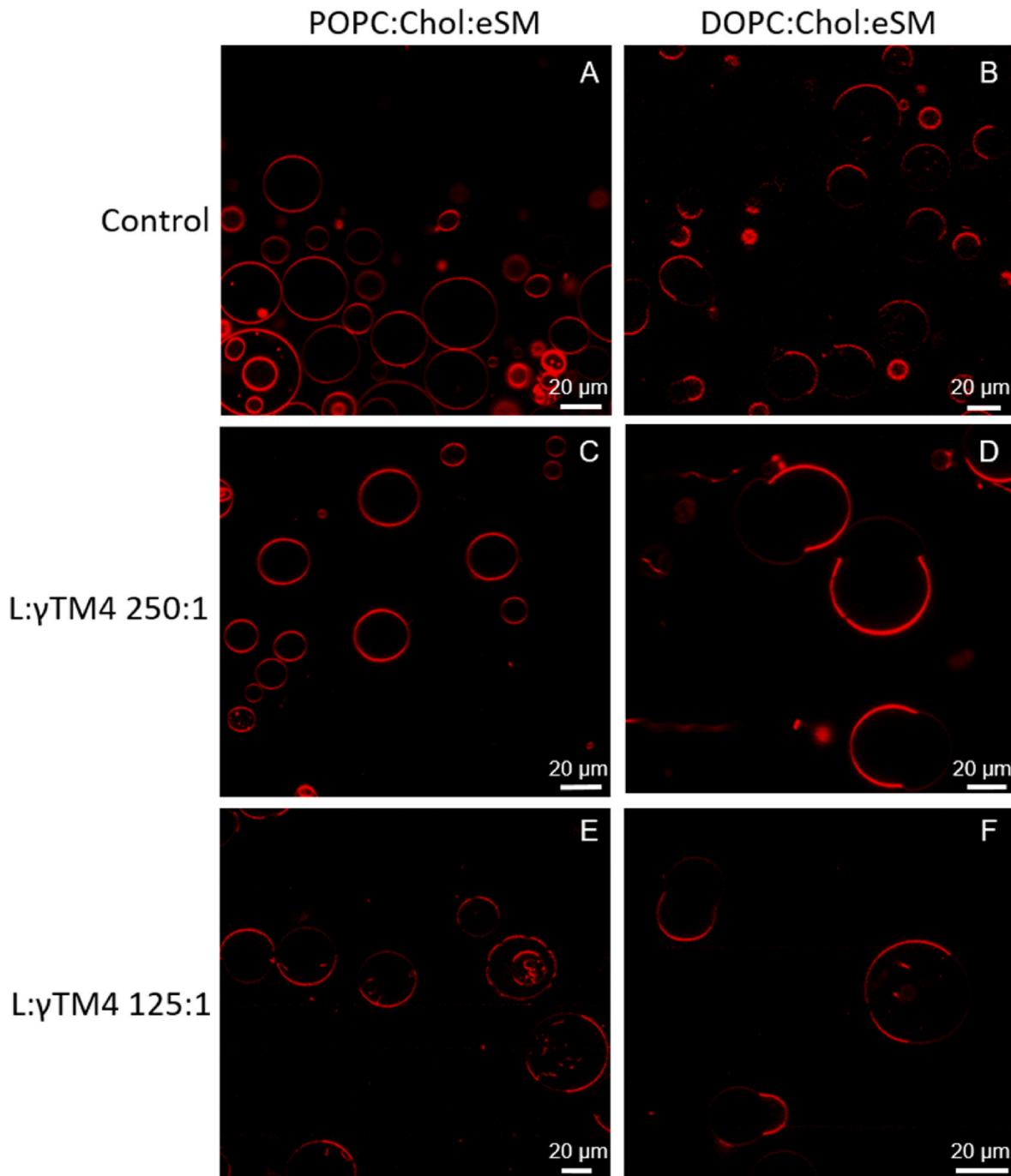

Fig. 5. Confocal microscopy of GUVs labeled with 0.1% DiI C-18. A) POPC:Chol:eSM (1:1:1), no phase separation is observed. B) DOPC:Chol:eSM (1:1:1) a coexistence of Lo and Ld domains is observed. C) POPC:Chol:eSM (1:1:1) + γTM4 250:1 L:P D) DOPC:Chol:eSM (1:1:1) + γTM4 250:1 L:P. E) POPC:Chol:eSM (1:1:1) + γTM4 125:1 L:P. F) DOPC:Chol:eSM (1:1:1) + γTM4 125:1 L:P.

125:1 (Fig. 5). GUVs at 250:1 L:P ratio were not phase separated, similarly to the control ones. However, at increased γTM4 fraction, namely at 125:1 L:P ratio, domains of different sizes and shapes were detected. The latter indicates that the peptide effectively caused a rearrangement of its surrounding lipids, which in turn results in changes of the membrane organization (from nanoscopic to microscopic domains).

In order to study whether the peptide is located either indistinctly in Lo and Ld domains or have preferences for a particular phase, the vesicles were then incubated with coumarin, a probe that emits fluorescence when it reacts with thiol groups (in this case those present in γTM4). POPC:Chol:eSM (1:1:1, homogeneous) and DOPC:Chol:eSM (1:1:1, phase-separated) vesicles were prepared with and without the peptide (L:P of 250:1) and were subsequently incubated with coumarin as a marker for the location of γTM4.

In POPC:Chol:eSM (1:1:1) GUVs containing γTM4, coumarin signal was hardly detected in the phospholipid bilayer (Fig. 6), whereas in phase separated DOPC:Chol:eSM (1:1:1) GUVs, with the same L:P ratio, coumarin signal was observed mainly in Ld domains (Fig. 6). This result may suggest that the peptide concentrates in these domains.

In order to investigate whether coumarin labels the membrane nonspecifically and to see if DiI-C18 and coumarin exhibit crosstalk, we performed additional control experiments. DOPC:Chol:eSM (1:1:1) vesicles with and without γTM4 were labeled with either DiI-C18 and coumarin or only with DiI-C18. GUVs were observed in the coumarin channel. Vesicles with or without γTM4 labeled only with DiI-C18 did not show any fluorescence signal (Fig. S4 B and C). In the case of vesicles containing both dyes, low fluorescence signal was detected even in the absence of the peptide (Fig. S4 D). However, the signal was much higher in the presence of γTM4, confirming that coumarin was located in Ld domains and effectively labeled the peptide (Fig. S4 A).

To gain insight into the changes of membrane organization observed in GUVs containing the γTM4 peptide, we then studied if the mere presence of the peptide can perturb the miscibility transition temperature of microscopically phase-separated DOPC:Chol:eSM (1:1:1) GUVs stained with DiI-C18 and containing γTM4 peptide (at 250:1 L:P ratio). We measured the miscibility behavior from temperature scans and defined the miscibility temperature as the one at which the fraction of phase separated vesicles is equal to that of homogeneous ones (see e.g. Ref. [51]). Fig. 7 shows an increment of the miscibility temperature in vesicles from $31.60 \pm 0.50 \,^{\circ}C$ (n = 3) for vesicles without the peptide to $36.88 \pm 0.18 \,^{\circ}C$ (n = 3) for membranes with the peptide, p = 5.8 × 10^{-5}. This increment confirms that the peptide effectively partitioned in the membrane attributing greater order of the lipids in Ld domains, which could be a consequence of either the presence of the peptide itself in these domains and/or a possible increment of Chol in Ld domains because of its affinity to γTM4.

To further understand these results, FRAP measurements were performed on DOPC:Chol:eSM (1:1:1) GUVs -with or without γTM4-labeled with DiI-C18. The diffusion of DiI-C18 in Ld domains significantly decreased in the presence of the peptide, and this behavior was dependent on the concentration of the peptide (L:P 250:1 or 125:1) (Fig. 8). Thus, all together, miscibility transition temperature measurements and FRAP experiments point to the fact that the mere presence of a protein component in the system alters the properties of the membrane, leading to a greater order.
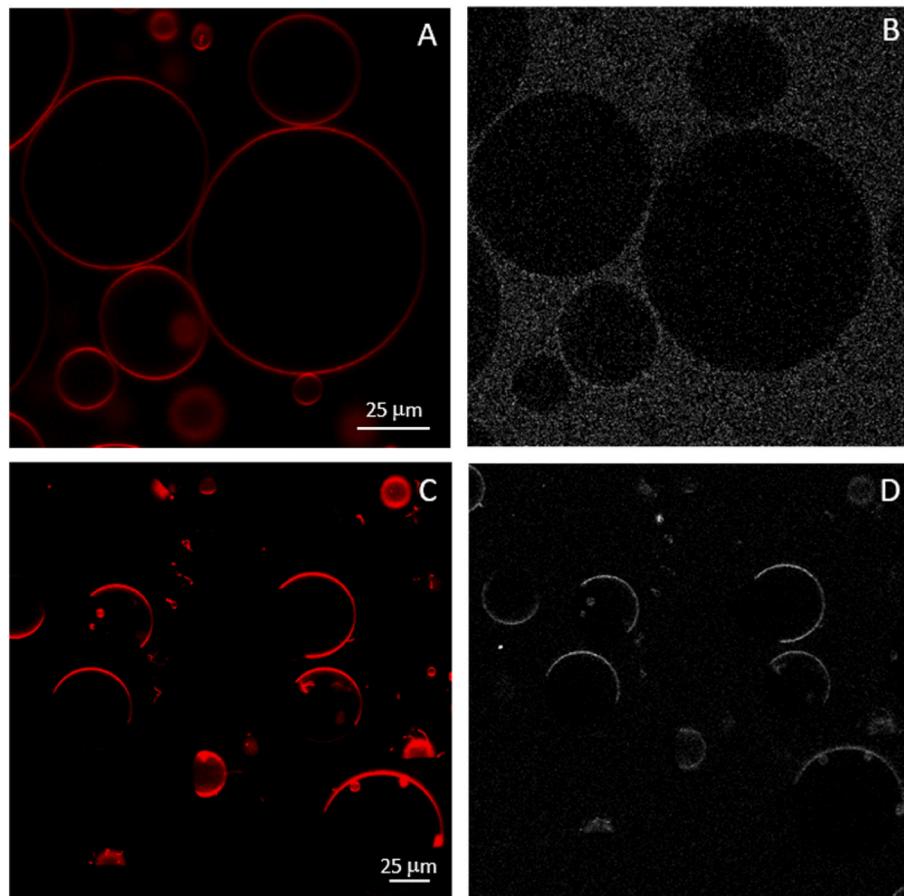

Fig. 6. Confocal microscopy of GUVs made of POPC:Chol:eSM (1:1:1) (A, B) and DOPC:Chol:eSM (1:1:1) (C, D) containing γTM4 250:1. A and C) show the DiI- C18 channel; B and D) show the coumarin channel.
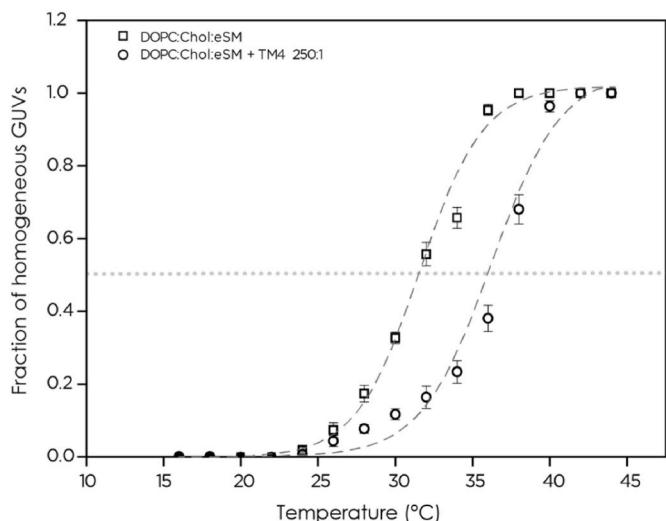
Fig. 7. Miscibility transition curves for DOPC:Chol:eSM (1:1:1) vesicles with (o) or without (□) γTM4 peptide (250:1 L:P). Data were fitted using the Boltzmann model and τ_{mix} was deduced from the half-maximum indicated by the dotted line. Error bars represent the standard error of the mean of three independent experiments.
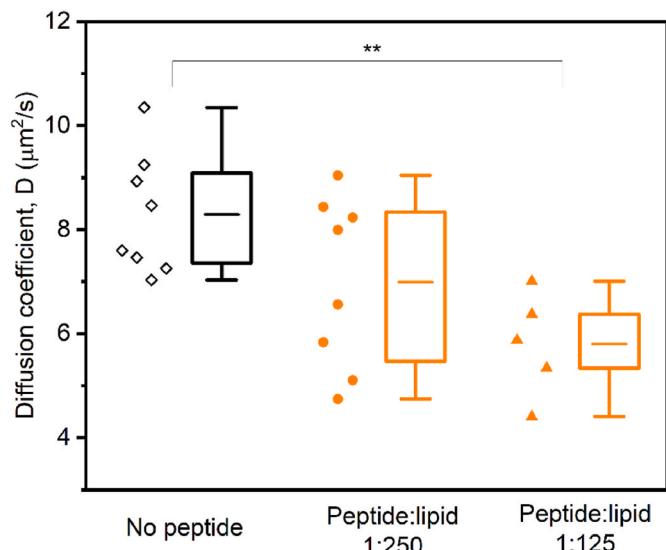

Fig. 8. Diffusion coefficients of DiI-C18 in DOPC:Chol:eSM (1:1:1) vesicles without (◇) or with γTM4 peptide at two different L:P ratios, 250:1 (●) or 125:1 (▲). Each symbol corresponds to a single measurement. P-value was determined by Student's t-test at the 0.05 level. **: $p < 0.01$.
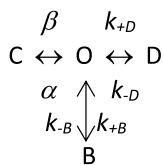
4. Discussion

Taking into account that the nAChR is a transmembrane protein, the properties of its lipid environment are essential for its conformation, activity, and function and also for its macromolecular organization and location in the membrane [21–25]. Lipids are present in different amounts in different membrane tissues, and they also vary during lifetime and in several neurodegenerative diseases, such as Alzheimer's disease [37,86]. In particular, Chol is a crucial lipid that conditions membrane organization, stability and fluidity, among other membrane properties. In this work, we studied the feasibility of a two-way communication process between γTM4 peptide, a representative model of the nAChR, and its surrounding membrane.

Three different variations of membrane Chol were explored: (i) an increment in the total amount of Chol, (ii) a sterol enrichment but in an asymmetric way by incorporation of CHEMS (which localizes mainly in the outer leaflet), and (iii) a same amount of sterol but with a change in Chol molecule as a result of an enzymatic oxidation by ChOx.

An increase in the total amount of Chol in the membrane did not correlate with a perturbation of membrane order. Previous studies postulated that in binary or ternary lipid systems, the presence of Chol affects the membrane order up to a maximum amount that corresponds to 33 mol%, in which a saturating effect is reached [72,87]. In our experiments, the initial Chol amount in vesicles and *T. californica* membranes was 33 mol% and ~35 mol%, respectively, which is why increasing the Chol fraction induced no changes in the membrane order. This could explain why no conformational changes were observed in nAChR-rich membranes from *T. californica* after Chol incorporation. Although the effect of the increment of Chol on the membrane order reaches a saturation state, it has been reported that it influences nAChR behavior. A Chol fraction of 33% in the membrane was reported as the optimum for nAChR activity [31,88]. An inhibition of ~52% of the macroscopic currents of nAChRs from *T. californica* was observed in *Xenopus laevis* oocytes when the Chol/phospholipid ratio was increased from 0.51 to 0.87 [89]. In another study, a reduction of 33% of the mean open time of the nAChR after incubation with Chol was reported [90]. More recently, Báez-Pagán et al. [91] showed that α7, α2β4, muscle nAChR, and nAChRs from *T. californica* expressed in *X. laevis* oocytes reduced their activity in direct relation with an increment of the Chol/phospholipid ratio. It has been previously proposed that an increment of Chol in the membrane not only relocates nAChRs to Chol-rich domains but also causes it to remain in a non-active state. In this work, we showed that an increment of Chol did induce perturbations in membrane organization and this could be related to nAChR function. GUVs composed of equimolar amounts of Chol, POPC and SM exhibit nanoscopic domains that are not visible by confocal microscopy [65], and this state was preserved when further Chol was added after GUVs formation (Fig. 4). However, when the vesicles were prepared with increased amount of Chol (POPC:Chol:bSM 1:2:1), coexistence of Lo and Ld domains was observed (Fig. 4). Considering that the membrane order remained the same (Table S1), it could be postulated that even though the number of Lo domains may increase, the membrane intensive properties also remain the same. The increment of Chol molecules in the initial lipid ratio resulted in bigger GUVs with a different microscopic lipid organization. Thus, an increment of Chol led to an increment in the amount of Lo domains that could be related to the previously postulated aggregation of nAChRs in them, which could constitute a pool of non-active receptors.

After the addition of CHEMS, a different response was observed. CHEMS is a Chol derivative with a negatively charged succinate group at pH 7.4 that concentrates in the external leaflet of the membrane near the lipid-water interface [48,92]. Both Chol and CHEMS caused a reduction of acyl chains mobility [92–94]. Depending on the lipid system under study, some studies propose that CHEMS has a major capacity to stabilize the lipid membrane than Chol [94], while others consider that it is Chol the one that has the greatest membrane ordering effect [45,92]. In this work, after incubation with CHEMS and contrary to what was observed with Chol, the membrane order increased both in nAChR-rich membranes and in synthetic LUVs (Table S1). Using DPH fluorescence anisotropy with POPC vesicles, Massey et al. [92] observed higher anisotropy changes in the presence of Chol than in the presence of CHEMS. However, they did not explore saturating concentrations of Chol as we did in the present work. The differences between Chol and CHEMS with respect to their impact on membrane order in model systems could also result in differences in lipid-protein interaction [45]. This could explain why after addition of CHEMS in the presence of a high concentration of carb we observed that the muscle nAChR does not get stabilized in a desensitized state but in a resting one (Fig. 1). Different explanations are plausible. Considering Scheme 1, one possibility is that the nAChR cannot respond to the agonist and remains in a resting state.

$$\begin{array}{ccc} \beta & & k_{+D} \\ C \leftrightarrow & O & \leftrightarrow D \\ \alpha & \uparrow & k_{-D} \\ k_{-B} & \downarrow k_{+B} \\ & B & \end{array}$$

Scheme 1. Minimal model for nAChR activation, desensitization and block.

Another possibility is that under this condition, the nAChR has a faster closing rate constant (α), which results in a faster return to a closed state instead of a stabilization in a desensitized one. A third possibility could be that CHEMS stabilizes the nAChR in a blocked state avoiding its desensitization.

Our patch-clamp experiments confirmed that the receptor is functional in the presence of CHEMS, which allowed us to discard the first possibility. From single-channel recordings we observed that events obtained in the presence of CHEMS display a reduced open duration with an increase in the area of the briefest closed state, thus suggesting that this compound could be modulating the receptor by the other two possibilities (either increasing its closing rate or acting as an open channel blocker). One experimental strategy to discriminate between both explanations could be to perform patch-clamp experiments increasing the concentration of CHEMS. However, it was not empirically possible to incorporate higher amounts of CHEMS considering its critical micellar concentration and the maximum time during which cells can be incubated with CHEMS. It is therefore interesting to consider some previous studies of our group in which we observed, by using CrV, different nAChR conformational states in the presence of: a) α-bungarotoxin, a nAChR competitive antagonist that stabilized the nAChR in a resting no-conducting state with a K_D value similar to that in the control resting state [55], b) QX-314, an ion channel blocker that stabilized the nAChR in a conformation different from the resting and the desensitized states, characterized by a higher K_D value than the one in the control resting state [55], and c) different free fatty acids (FFA) inside the membrane which conducted the nAChR to distinct conformational states depending on each FFA [57] with K_D values between the control resting and desensitized states, i.e. cis 18:1, which behaves as a nAChR allosteric antagonist through the receptor transmembrane region, carries the nAChR to a desensitized state [57]. Comparing results from the present work with the above-mentioned ones, it is possible to assume that the perturbation caused by CHEMS in the membrane order (Table S1) and the differential lipid distribution between both leaflets (Fig. S2) alter nAChR activation equilibrium favoring a rapid return to a resting conformation from the open state. Even though neither the addition of CHEMS to GUVs composed of an equimolar amount of Chol, POPC, and SM nor POPC:Chol:CHEMS:bSM (1:1:1:1) GUVs showed microscopic Lo domains, although the increment of CHEMS molecules in the initial lipid ratio resulted in bigger GUVs, and taking into account that after the addition of this lipid the membrane order was increased (Table S1), possibly the nanoscopic Lo and Ld domains changed their intensive biophysical properties, which could explain the altered nAChR function. The differences between CHEMS and Chol can be explained taking into account that while Chol localizes in both leaflets and forms Lo domains, CHEMS tends to localize only in the outer leaflet and forms domains different from those observed in the presence of Chol. Recently, by crioelectromicroscopy of *Torpedo* nAChR, Rahman et al. (2022) showed Chol molecules at low affinity binding sites located in the outer hemilayer, and they also located the activation gate at the extracellular half of the pore [13]. Our results reinforce this observation, thus demonstrating that perturbation of Chol in the outer leaflet perturbs nAChR function (causing a loss of function).

Finally, the enzymatic transformation of Chol into cholestenone caused no membrane order perturbations (Table S1). Jafurulla et al. [95] observed that a reduction of ~45% of the membrane Chol by ChOx caused no changes in the membrane order and concluded that although the enzyme oxidizes one hydroxyl group per Chol molecule, the main Chol structure remains the same. Furthermore, although ChOx binds to the surface of the outer leaflet [96], both Chol and cholestenone have a rapid *trans*-bilayer motion (flip-flop) so that ChOx action induces no further transbilayer asymmetry [82]. However, contrary to what happens with Chol, in model systems cholestenone localizes mainly in Ld domains [79–81] and therefore treatment with ChOx disrupts Chol-rich membrane domains [82]. When GUVs of POPC:Chol:bSM (1:1:1) were treated with ChOx, big microscopic Lo domains were observed (Fig. 4) probably because the disruption of Lo, and the consequent lipid rearrangement, induced new ordered and disordered domains producing their coalescence, and thereby Ld and Lo domains changed their intensive biophysical properties. This deviation from the control condition could probably explain why after the treatment with ChOx and in the presence of high concentrations of carb, we observed that the nAChR did not stabilize in a desensitized state but in a resting one (Fig. 1). Although this behavior was apparently similar to that observed after CHEMS addition, patch-clamp experiments showed noticeable differences. Single-channel recordings showed that after incubation with ChOx, nAChR activity was similar to that under the control condition (Fig. 2). However, macroscopic currents in the whole-cell configuration showed that the nAChR spent less time in the desensitized state, probably due to a higher k_{-D} constant than that under the control condition (Scheme 1, Fig. 3) [97]. After the oxidation of Chol to cholestenone, the nAChR recovered from desensitization more rapidly than under the control condition. A diminished latency and faster recovery from desensitization can be considered as a gain of nAChR function. Rahman et al. (2022) showed a high affinity site for Chol in the inner leaflet near the MX helix next to where they also postulated the occurrence of a desensitization gate (close to the cytoplasmic hole of the channel) [13]. They also demonstrated that point mutations at the cytoplasmic site resulted in a gain of function with a rapid recovery from desensitization, assigning a functional role of this mechanism to M4 [13]. In the present work, we demonstrated that perturbations of Chol mainly at this level also lead to a rapid recovery from desensitization, confirming the intimate relationship between lipids and the receptor. According to Rahman et al. (2022), the above-mentioned changes in the lipid microenvironment alter M4 stability, thus affecting nAChR function [13].

The treatment with ChOx did not perturb the overall membrane order of the model systems (Table S1) but it did perturb the membrane structure, with an increment of Ld domains, and caused a change of nAChR equilibrium producing a more rapid rate of recovery after desensitization with a gain of nAChR function (Fig. 3). The recovery from desensitization showed a dependency on the structure of Chol, which points to a more specific location. These results are opposite to those obtained after addition of CHEMS, which showed a change of the intensive properties of Lo domains and a diminished function of the nAChR. Altogether, these results reinforce the importance of the nAChR microenvironment (asymmetry, composition or membrane order) for a proper nAChR gating and desensitization, and, in particular, the crucial role of Chol molecules at different locations. Furthermore, these results highlight the importance of using complementary techniques to understand molecular mechanisms because neither CrV studies nor patch clamp studies alone could have allowed us to interpret the effect of Chol changes on nAChR function.

Taking into account that changes in membrane Chol lead to changes not only in nAChR function and location but also in membrane organization, we studied if changes in the amount of γTM4 peptide have an impact on membrane order and/or organization. The γTM4 peptide is a synthetic peptide that i) is representative of the most exposed receptor transmembrane segment to the lipid microenvironment, ii) is considered a nAChR lipid sensor [13,14], and iii) is related to nAChR desensitization [13,14]. To this end, GUVs with two different lipid compositions that present either microscopically homogeneous membrane (with nanoscopic domains) or a microscopic coexistence of Ld/Lo domains were used. The first evidence of the interaction between the peptide and

its surrounding lipids was the perturbation of the membrane organization evidenced by the change of nanoscopic domains to microscopic ones when the L:P ratio was 125:1 (Fig. 5). A striking finding was that, in contrast to previous results, in the system already exhibiting microscopic domains, the peptide partitioned predominantly in the Ld phase (Fig. 6) [98]. Only if GUVs had microscopic domains it could be possible to observe the fluorescence of the peptide in the membrane. This could be due to the fact that coumarin has access only to those peptides that are located in a fluid environment and therefore in either Lo domains or in systems with nanoscopic domains where coumarin is not effective because Lo and Ld domains are very close to each other. Furthermore, upon partitioning in the microscopic domains, the peptide becomes more concentrated in them, thus enhancing the signal. In this respect, the fact that the γTM4 peptide was observed mainly in Ld domains does not discard the possibility that this peptide is also in the Lo phase. In addition, Bermudez et al. [98] found the peptide mainly in DRM (detergent resistant membranes) after treating the LUVs of POPC:Chol: SM (1:1:1) containing γTM4 (250:1 L:P) with Triton X-100. However, this different location may respond to an artifactual effect caused by the perturbation of the membrane organization and peptide distribution due to the presence of detergent. Finally, we observed that Ld domains of GUVs with microscopic domains coexistence changed their intensive properties in the presence of the peptide (250:1 L:P), increasing their membrane order (higher miscibility temperature and lower diffusion coefficient than in the absence of the peptide, Figs. 7 and 8). This is not only a confirmation of i) the presence of the peptide in these domains and/or ii) the migration of Chol molecules to these domains, possibly due to their affinity to the peptide, but also a strong demonstration of the intimate relationship between protein and lipid entities within the membrane.

In this work, we showed that there is a two-way communication process between nAChR and its surrounding membrane. We correlated the crucial role of Chol in maintaining a proper membrane order and organization and its location at distinct sites in the lipid microenvironment with nAChR function. In parallel, we demonstrated that γTM4, a minimalist and yet representative model of the nAChR to which a lipid sensor role can be attributed, can generate significant perturbations of the surrounding lipids, inducing changes in membrane organization and in its biophysical intensive properties. Altogether, we here demonstrated a feedback relationship between membrane organization and nAChR function, i.e. whereas the presence of a model of nAChRs conditions the membrane organization, changing the lipid microenvironment, membrane organization and composition perturb nAChRs function. Taken together, our results lead to the conclusion that nAChRs have a gain of function in disordered membrane environments (i.e. after ChOx treatment) and a loss of function in ordered ones (i.e. after CHEMS or Chol treatments). This is congruent with the fact that γTM4 not only localizes mainly in Ld domains but also conditions its order environment in this way. Finally, we demonstrated that Chol molecules at the outer leaflet (CHEMS experiments) in annular sites and at the inner leaflet (ChOx experiments) in non-annular sites are related to nAChR gating and desensitization, respectively.

Acknowledgements

Appendix A. Supplementary data

Supplementary data to this article can be found online at https://doi.org/10.1016/j.abb.2022.109413.

References

[1] A. Karlin, M.H. Akabas, Toward a structural basis for the function of nicotinic acetylcholine receptors and their cousins, Neuron 6 (1995) 1231–1244, https://doi.org/10.1016/0896-6273(95)90004-7.

[2] N. Le Novère, J.P. Changeux, Molecular evolution of the nicotinic acetylcholine receptor: an example of multigene family in excitable cells, J. Mol. Evol. 40 (1995) 155–172, https://doi.org/10.1007/BF00167110.

[3] J.P. Changeux, S.J. Edelstein, Allosteric receptors after 30 years, Neuron 5 (1998) 959–980, https://doi.org/10.1016/s0896-6273(00)80616-9.

[4] D. Paterson, A. Nordberg, Neuronal nicotinic receptors in the human brain, Prog. Neurobiol. 61 (2000) 75–111, https://doi.org/10.1016/s0301-0082(99)00045-3.

[5] N. Unwin, Refined structure of the nicotinic acetylcholine receptor at 4A resolution, J. Mol. Biol. 346 (2005) 967–989, https://doi.org/10.1016/j.jmb.2004.12.031.

[6] S.S. Antollini, Y. Xu, H. Jiang, F.J. Barrantes, Fluorescence and molecular dynamics studies of the acetylcholine receptor gammaM4 transmembrane peptide in reconstituted systems, Mol. Membr. Biol. 22 (2005) 471–483, https://doi.org/10.1080/09687860500367915.

[7] J.E. Baenziger, P.J. Corringer, 3D structure and allosteric modulation of the transmembrane domain of pentameric ligand-gated ion channels, Neuropharmacology 60 (2011) 116–125, https://doi.org/10.1016/j.neuropharm.2010.08.007.

[8] J.E. Baenziger, C.J.B. DaCosta, Molecular mechanisms of acetylcholine receptor-lipid interactions: from model membranes to human biology, Biophys. Rev. 5 (2013) 1–9, https://doi.org/10.1007/s12551-012-0078-7.

[9] F.J. Barrantes, Phylogenetic conservation of protein-lipid motifs in pentameric ligand-gated ion channels, Biochim. Biophys. Acta 1848 (2015) 1796–1805, https://doi.org/10.1016/j.bbamem.2015.03.028.

[10] J. Corradi, C. Bouzat, Understanding the bases of function and modulation of α7 nicotinic receptors: implications for drug discovery, Mol. Pharmacol. 90 (2016) 288–299, https://doi.org/10.1124/mol.116.104240.

[11] C.L. Morales-Pérez, C.M. Noviello, R.E. Hibbs, X-ray structure of the human α4β2 nicotinic receptor, Nature 538 (2016) 411–415, https://doi.org/10.1038/nature19785.

[12] N.L. Absalom, P.R. Schofield, T.M. Lewis, Pore structure of the Cys-loop ligand-gated ion channels, Neurochem. Res. 34 (2009) 1805–1815, https://doi.org/10.1007/s11064-009-9971-2.

[13] M. Rahman, T. Basta, J. Teng, M. Lee, B.T. Worrell, M.H.B. Stowell, R.E. Hibbs, Structural mechanism of muscle nicotinic receptor desensitization and block by curare, Nat. Struct. Mol. Biol. 29 (2022) 386–394, https://doi.org/10.1038/s41594-022-00737-3.

[14] F.J. Barrantes, V. Bermudez, M.V. Borroni, S.S. Antollini, M.F. Pediconi, J.C. Baier, I. Bonini, C. Gallegos, A.M. Roccamo, A.S. Valles, V. Ayala, C. Kamerbeek, Boundary lipids in the nicotinic acetylcholine receptor microenvironment, J. Mol. Neurosci. 40 (2010) 87–90, https://doi.org/10.1007/s12031-009-9262-z.

[15] C. Bouzat, New insights into the structural bases of activation of Cys-loop receptors, J. Physiol. Paris 106 (2012) 23–33, https://doi.org/10.1016/j.jphysparis.2011.09.012.

[16] J. Lindstrom, Autoimmune diseases involving nicotinic receptors, J. Neurobiol. 53 (2002) 656–665, https://doi.org/10.1002/neu.10106.

[17] B.E. McKay, A.N. Placzek, J.A. Dani, Regulation of synaptic transmission and plasticity by neuronal nicotinic acetylcholine receptors, Biochem. Pharmacol. 74 (2007) 1120–1133, https://doi.org/10.1016/j.bcp.2007.07.001.

[18] M. Pohanka M, Cholinesterases, a target of pharmacology and toxicology, Biomed. Pap. Med. Fac. Univ. Palacky. Olomouc. Czech. Repub. 155 (2012) 219–229, https://doi.org/10.5507/bp.2011.036.

[19] C. Bouzat, M. Lasala, B.E. Nielsen, J. Corradi, M.D.C. Esandi, Molecular function of alpha7 nicotinic receptors as drug targets, J. Physiol. 596 (2018) 1847–1861, https://doi.org/10.1113/JP275101.

[20] E.X. Albuquerque, E.F. Pereira, M. Alkondon, S.W. Rogers, Mammalian nicotinic acetylcholine receptors: from structure to function, Physiol. Rev. 89 (2009) 73–120, https://doi.org/10.1007/s10254-003-0005-1.

[21] F.J. Barrantes, Structural basis for lipid modulation of nicotinic acetylcholine receptor function, Brain Res. Rev. 47 (2004) 71–95, https://doi.org/10.1016/j.brainresrev.2004.06.008.

[22] C.J. DaCosta, I.D. Wagg, M.E. McKay, J.E. Baenziger, Phosphatidic acid and phosphatidylserine have distinct structural and functional interactions with the nicotinic acetylcholine receptor, J. Biol. Chem. 279 (2004) 14967–14974, https://doi.org/10.1074/jbc.M310037200.

[23] M.F. Pediconi, C.E. Gallegos, E.B. De Los Santos, F.J. Barrantes, Metabolic cholesterol depletion hinders cell-surface trafficking of the nicotinic acetylcholine receptor, Neuroscience 128 (2004) 239–249, https://doi.org/10.1016/j.neuroscience.2004.06.007.

[24] C.J. Baier, F.J. Barrantes, Sphingolipids are necessary for nicotinic acetylcholine receptor export in the early secretory pathway, J. Neurochem. 101 (2007) 1072–1084, https://doi.org/10.1111/j.1471-4159.2007.04561.x.

[25] J.E. Baenziger, C.M. Hénault, J.P. Therien, J. Sun, Nicotinic acetylcholine receptor-lipid interactions: mechanistic insight and biological function, Biochim. Biophys. Acta 1848 (2015) 1806–1817, https://doi.org/10.1016/j.bbamem.2015.03.010.

[26] D. Marsh, F.J. Barrantes, Immobilized lipid in acetylcholine receptor-rich membranes from Torpedo marmorata, Proc. Natl. Acad. Sci. U.S.A. 75 (1978) 4329–4333, https://doi.org/10.1073/pnas.75.9.4329.

[27] O.T. Jones, M. McNamee, Annular and nonannular binding sites for cholesterol associated with the nicotinic acetylcholine receptor, Biochemistry 27 (1988) 2364–2374, https://doi.org/10.1021/bi00407a018.

[28] S.S. Antollini, M.A. Soto, I. Bonini, C. Gutiérrez-Merino, P. Sotomayor, F. J. Barrantes, Physical state of bulk and protein-associated lipid in nicotinic acetylcholine receptor-rich membrane studied by laurdan generalized polarization and fluorescence energy transfer, Biophys. J. 70 (1996) 1275–1284, https://doi.org/10.1016/S0006-3495(96)79684-4.

[29] S.S. Antollini, F.J. Barrantes, Disclosure of discrete sites for phospholipid and sterols at the protein-lipid interface in native acetylcholine receptor-rich membrane, Biochemistry 37 (1998) 16653–16662, https://doi.org/10.1021/bi9808215.

[30] S.B. Mantipragada, L.I. Horváth, H.R. Arias, G. Schwarzmann, K. Sandhoff, F. J. Barrantes, D. Marsh D, Lipid-protein interactions and effect of local anesthetics in acetylcholine receptor-rich membranes from Torpedo marmorata electric organ, Biochemistry 42 (2003) 9167–9175, https://doi.org/10.1021/bi034485q.

[31] A.K. Hamouda, D.C. Chiara, D. Sauls, J.B. Cohen, M.P. Blanton, Cholesterol interacts with transmembrane alpha-helices M1, M3, and M4 of the Torpedo nicotinic acetylcholine receptor: photolabeling studies using [3H]Azicholesterol, Biochemistry 45 (2006) 976–986, https://doi.org/10.1021/bi051978h.

[32] G.A. Fernández Nievas, F.J. Barrantes, S.S. Antollini, Modulation of nicotinic acetylcholine receptor conformational state by free fatty acids and steroids, J. Biol. Chem. 283 (2008) 21478–21486, https://doi.org/10.1074/jbc.M800345200.

[33] A.G. Lee, Lipid-protein interactions in biological membranes: a structural perspective, Biochem. Biophys. Acta. 1612 (2003) 1–40, https://doi.org/10.1016/s0005-2736(03)00056-7.

[34] C. Bechara, C.V. Robinson, Different modes of lipid binding to membrane proteins probed by mass spectrometry, J. Am. Chem. Soc. 137 (2015) 5240–5247, https://doi.org/10.1021/jacs.5b00420.

[35] M. Landreh, M.T. Marty, J. Gault, C.V. Robinson, A sliding selectivity scale for lipid binding to membrane proteins, Curr. Opin. Struct. Biol. 39 (2016) 54–60, https://doi.org/10.1016/j.sbi.2016.04.005.

[36] J.R. Bolla, R.A. Corey, C. Sahin, J. Gault, A. Hummer, J.T.S. Hopper, D.P. Lane, D. Drew, T.M. Allison, P.J. Stansfeld, C.V. Robinson, M. Landreh, A mass-spectrometry-based approach to distinguish annular and specific lipid binding to membrane proteins, Angew. Chem., Int. Ed. Engl. 59 (2020) 3523–3528, https://doi.org/10.1002/anie.201914411.

[37] R.S. Yadav, N.K. Tiwari, Lipid integration in neurodegeneration: an overview of Alzheimer's disease, Mol. Neurobiol. 50 (2014) 168–176, https://doi.org/10.1007/s12035-014-8661-5.

[38] C.P. Schaaf, Nicotinic acetylcholine receptors in human genetic disease, Genet. Med. 16 (2014) 649–656, https://doi.org/10.1038/gim.2014.9.

[39] V. Narayanaswami, M.G. McNamee, Protein-lipid interactions and Torpedo californica nicotinic acetylcholine receptor function. 2. Membrane fluidity and ligand-mediated alteration in the accessibility of gamma subunit cysteine residues to cholesterol, Biochemistry 32 (1993) 12420–12427.

[40] G. Brannigan, J. Hénin, R. Law, R. Eckenhoff, M.L. Klein, Embedded cholesterol in the nicotinic acetylcholine receptor, Proc. Natl. Acad. Sci. USA 105 (2008) 14418–14423, https://doi.org/10.1016/bs.ctm.2017.05.001.

[41] G. Brannigan G, Direct interactions of cholesterol with pentameric ligand-gated ion channels: testable hypotheses from computational predictions, Curr. Top. Membr. 80 (2017) 163–186, https://doi.org/10.1016/bs.ctm.2017.06.002.

[42] N. Unwin, Protein-lipid architecture of a cholinergic postsynaptic membrane, IUCRJ 28 (2020) 852–859, https://doi.org/10.1107/S2052252520009446.

[43] C.J. Baier, J. Fantini, F.J. Barrantes, Disclosure of cholesterol recognition motifs in transmembrane domains of the human nicotinic acetylcholine receptor, Sci. Rep. 1 (2011) 69, https://doi.org/10.1038/srep00069.

[44] J. Fantini, C. Di Scala, C.J. Baier, F.J. Barrantes, Molecular mechanisms of protein-cholesterol interactions in plasma membranes: functional distinction between topological (tilted) and consensus (CARC/CRAC) domains, Chem. Phys. Lipids 199 (2016) 52–60, https://doi.org/10.1016/j.chemphyslip.2016.02.009.

[45] W. Kulig, J. Tynkkynen, M. Javanainen, M. Manna, T. Rog, I. Vattulainen, P. Jungwirth, How well does cholesteryl hemisuccinate mimic cholesterol in saturated phospholipid bilayers? J. Mol. Model. 20 (2014) 2121, https://doi.org/10.1007/s00894-014-2121-z.

[46] N.S. Sampson Ns, Dissection of a flavoenzyme active site: the reaction catalyzed by cholesterol oxidase, Antioxidants Redox Signal. 3 (2001) 839–846, https://doi.org/10.1089/15230860152665019.

[47] N.S. Sampson, A. Vrielink, Cholesterol oxidases: a study of nature's approach to protein design, Acc. Chem. Res. 36 (2003) 713–722, https://doi.org/10.1021/ar9800587.

[48] P.I. Lario, N. Sampson, A.J. Vrielink A.J, Sub-atomic resolution crystal structure of cholesterol oxidase: what atomic resolution crystallography reveals about enzyme mechanism and the role of the FAD cofactor in redox activity, Mol. Biol. 326 (2011) 1635–1650, https://doi.org/10.1016/s0022-2836(03)00054-8.

[49] F.J. Barrantes, Oligomeric forms of the membrane-bound acetylcholine receptor disclosed upon extraction of the Mr 43,000 nonreceptor peptide, J. Cell Biol. 92 (1982) 60–68, https://doi.org/10.1083/jcb.92.1.60.

[50] E.G. Bligh, W.J. Dyer, A rapid method of total lipid extraction and purification, Can. J. Biochem. Physiol. 37 (1959) 911–917.

[51] B. Kubsch, T. Robinson, R. Lipowsky, R. Dimova, Solution asymmetry and salt expand fluid-fluid coexistence regions of charged membranes, Biophys. J. 110 (2016) 2581–2584, https://doi.org/10.1016/j.bpj.2016.05.028.

[52] B. Kubsch, T. Robinson, J. Steinkühler, R. Dimova, Phase behavior of charged vesicles under symmetric and asymmetric solution conditions monitored with fluorescence microscopy, JoVE 24 (2017), 56034, https://doi.org/10.3791/56034.

[53] M. Kang, C.A. Day, A.K. Kenworthy, E. DiBenedetto, Simplified equation to extract diffusion coefficients from confocal FRAP data, Traffic 13 (2012) 1589–1600, https://doi.org/10.1111/tra.12008.

[54] R.B. Lira, J. Steinkühler, R.L. Knorr, R. Dimova, K.A. Riske, Posing for a picture: vesicle immobilization in agarose gel, Sci. Rep. 6 (2016), 25254, https://doi.org/10.1038/srep25254.

[55] C. Fabiani, A.P. Murray, J. Corradi, S.S. Antollini, A novel pharmacological activity of caffeine in the cholinergic system, Neuropharmacology 135 (2018) 464–473, https://doi.org/10.1016/j.neuropharm.2018.03.041.

[56] T. Parasassi, G. De Stasio, G. Ravagnan, R.M. Rusch, E. Gratton, Quantitation of lipid phases in phospholipid vesicles by the generalized polarization of Laurdan fluorescence, Biophys. J. 60 (1991) 179–189, https://doi.org/10.1016/S0006-3495(91)82041-0.

[57] V.L. Perillo, G.A. Fernández-Nievas, A.S. Vallés, F.J. Barrantes, S.S. Antollini, The position of the double bond in monounsaturated free fatty acids is essential for the inhibition of the nicotinic acetylcholine receptor, Biochim. Biophys. Acta 1818 (2012) 2511, https://doi.org/10.1016/j.bbamem.2012.06.001, 2220.

[58] M. Shinitzky, I. Yuli, Lipid fluidity at the submacroscopic level: determination by fluorescence polarization, Chem. Phys. Lipids 30 (1982) 261–282.

[59] C. Bouzat, N. Bren, S.M. Sine, Structural basis of the different gating kinetics of fetal and adult acetylcholine receptors, Neuron 13 (1994) 1395–1402, https://doi.org/10.1016/0896-6273(94)90424-3.

[60] J. Corradi, G. Spitzmaul, M.J. De Rosa, M. Costabel, C. Bouzat, Role of pairwise interactions between M1 and M2 domains of the nicotinic receptor in channel gating, Biophys. J. 92 (2007) 76–86, https://doi.org/10.1529/biophysj.106.088757.

[61] F. Qin, A. Auerbach, F. Sachs, Estimating single channel kinetic parameters from idealized patch-clamp data containing missed events, Biophys. J. 70 (1996) 264–280, https://doi.org/10.1016/s0006-3495(96)79568-1.

[62] F. Qin, A. Auerbach, F. Sachs, Maximum likelihood estimation of aggregated Markov processes, Proc. Roy. Soc. Lond. 264 (1997) 375–383, https://doi.org/10.1098/rspb.1997.0054.

[63] Y. Liu, J.P. Dilger Jp, Opening rate of acetylcholine receptor channels, Biophys. J. 60 (1991) 424–432, https://doi.org/10.1016/S0006-3495(91)82068-9.

[64] C.J.B. daCosta, C.R. Free, J. Corradi, C. Bouzat, S.M. Sine, Single-channel and structural foundations of neuronal α7 acetylcholine receptor potentiation, J. Neurosci. 31 (2011) 13870–13879, https://doi.org/10.1523/jneurosci.2652-11.2011.

[65] R.S. Petruzielo, F.A. Heberle, P. Drazba, J. Katsaras, G.W. Feigenson, Phase behavior and domain size in sphingomyelin-containing lipid bilayers, Biochim. Biophys. Acta 1828 (2013) 1302–1313, https://doi.org/10.1016/j.bbamem.2013.01.007.

[66] J. Lee, B.R. Lentz, Outer leaflet-packing defects promote poly(ethylene glycol)-mediated fusion of large unilamellar vesicles, Biochemistry 36 (1997) 421–431, https://doi.org/10.1021/bi9622332.

[67] B. Lentz, Use of fluorescent probes to monitor molecular order and motions within liposome bilayers, Chem. Phys. Lipids 64 (1993) 99–116, https://doi.org/10.1016/0009-3084(93)90060-g.

[68] W. Seel, D. Baust, D. Sons, M. Albers, L. Etzbach, J. Fuss, A. Lipski, Carotenoids are used as regulators for membrane fluidity by Staphylococcus xylosus, Sci. Rep. 10 (2020) 330, https://doi.org/10.1038/s41598-019-57006-5.

[69] S. Jaikishan, A. Björkbom, J.P. Slotte, Phosphatidyl alcohols: effect of head group size on domain forming properties and interactions with sterols, Biochim. Biophys. Acta 1798 (2010) 1615–1622, https://doi.org/10.1016/j.bbamem.2010.03.022.

[70] F.M. Harris, K.B. Best, J.D. Bell, Use of laurdan fluorescence intensity and polarization to distinguish between changes in membrane fluidity and phospholipid order, Biochim. Biophys. Acta 1565 (2002) 123–128, https://doi.org/10.1016/s0005-2736(02)00514-x.

[71] M.A. Soto-Arriaza, C. Olivares-Ortega, F.H. Quina, L.F. Aguilar, C.P. Sotomayor, Effect of cholesterol content on the structural and dynamic membrane properties of DMPC/DSPC large unilamellar bilayers, Biochim. Biophys. Acta 1828 (2013) 2763–2769, https://doi.org/10.1016/j.bbamem.2013.07.031.

[72] S.S. Antollini, F.J. Barrantes, Disclosure of discrete sites for phospholipid and sterols at the protein-lipid interface in native acetylcholine receptor-rich membrane, Biochemistry 37 (1998) 16653–16662, https://doi.org/10.1021/bi9808215.

[73] M.M. Lurtz, S.E. Pedersen, Aminotriarylmethane dyes are high-affinity noncompetitive antagonists of the nicotinic acetylcholine receptor, Mol. Pharmacol. 55 (1999) 159–167, https://doi.org/10.1124/mol.55.1.159.

[74] C. Bouzat, F.J. Barrantes, S. Sine, Nicotinic receptor fourth transmembrane domain: hydrogen bonding by conserved threonine contributes to channel gating kinetics, J. Gen. Physiol. 115 (2000) 663–672, https://doi.org/10.1085/jgp.115.5.663.

[75] H.R. Arias, P. Bhumireddy, C. Bouzat, Molecular mechanisms and binding site locations for noncompetitive antagonists of nicotinic acetylcholine receptors, Int. J. Biochem. Cell Biol. 38 (2006) 1254–1276, https://doi.org/10.1016/j.biocel.2006.01.006.

[76] R. Dimova, C.M. Marques, The Giant Vesicle Book, first ed., 2019. Boca Raton.

[77] R. Dimova, Giant vesicles and their use in assays for assessing membrane phase state, curvature, mechanics, and electrical properties, Annu. Rev. Biophys. 48 (2019) 93–119, https://doi.org/10.1146/annurev-biophys-052118-115342.

[78] V.L. Perillo, D.A. Peñalva, A.J. Vitale, F.J. Barrantes, S.S. Antollini, Transbilayer asymmetry and sphingomyelin composition modulate the preferential membrane partitioning of the nicotinic acetylcholine receptor in Lo domains, Arch. Biochem. Biophys. 591 (2016) 76–86, https://doi.org/10.1016/j.abb.2015.12.003.

[79] X. Xu, E. London, The effect of sterol structure on membrane lipid domains reveals how cholesterol can induce lipid domain formation, Biochemistry 39 (2000) 843–849, https://doi.org/10.1021/bi992543v.

[80] A.V. Samsonov, I. Mihalyov, F.S. Cohen, Characterization of cholesterol-sphingomyelin domains and their dynamics in bilayer membranes, Biophys. J. 81 (2001) 1486–1500, https://doi.org/10.1016/S0006-3495(01)75803-1.

[81] A.K. Rouquette-Jazdanian, C. Pelassy, J.P. Breittmayer, C. Aussel, Revaluation of the role of cholesterol in stabilizing rafts implicated in T cell receptor signalling, Cell. Signal. 18 (2006) 105–122.

[82] M. Neuvonen, M. Manna, S. Mokkila, M. Javanainen, T. Rog, Z. Liu, R. Bittman, I. Vattulainen, E. Ikonen, Enzymatic oxidation of cholesterol: properties and functional effects of cholestenone in cell membranes, PLoS One 9 (2014), e103743, https://doi.org/10.1371/journal.pone.0103743.eCollection.2014.

[83] J. Zhao, J. Wu, F.A. Heberle, T.T. Mills, P. Klawitter, G. Huang, G. Costanza, G. W. Feigenson, Phase studies of model biomembranes: complex behavior of DSPC/DOPC/cholesterol, Biochim. Biophys. Acta 1768 (2007) 2764–2776, https://doi.org/10.1016/j.bbamem.2007.07.008.

[84] N. Bezlyepkina, R.S. Gracià, P. Shchelokovskyy, R. Lipowsky, R. Dimova, Phase diagram and tie-line determination for the ternary mixture DOPC/eSM/cholesterol, Biophys. J. 104 (2013) 1456–1464, https://doi.org/10.1016/j.bpj.2013.02.024.

[85] A. Tsamaloukas, H. Szadkowska, H. Heerklotz, Nonideal mixing in multicomponent lipid/detergent systems, J. Phys. Condens. Matter 18 (2006) 1125–1138, https://doi.org/10.1088/0953-8984/18/28/S02.

[86] C. Fabiani, S.S. Antollini, Alzheimer's disease as a membrane disorder: spatial cross-talk among beta-amyloid peptides, nicotinic acetylcholine receptors and lipid rafts, Front. Cell. Neurosci. 13 (2019) 309, https://doi.org/10.3389/fncel.2019.00309.

[87] P.L. Chong, W. Zhu, B. Venegas, On the lateral structure of model membranes containing cholesterol, Biochim. Biophys. Acta 1788 (2009) 2–11.

[88] S.E. Rankin, G.H. Addona, M.A. Kloczewiak, B. Bugge, K.W. Miller, The cholesterol dependence of activation and fast desensitization of the nicotinic acetylcholine receptor, Biophys. J. 73 (1997) 2446–2455, https://doi.org/10.1016/S0006-3495(97)78273-0.

[89] J. Santiago, G.R. Guzmàn, L.V. Rojas, R. Marti, G.A. Asmar-Rovira, L.F. Santana, M. McNamee, J.A. Lasalde-Dominicci, Probing the effects of membrane cholesterol in the Torpedo californica acetylcholine receptor and the novel lipid-exposed mutation alpha C418W in Xenopus oocytes, J. Biol. Chem. 276 (2001) 46523–46532, https://doi.org/10.1074/jbc.M104563200.

[90] V. Borroni, C.J. Baier, T. Lang, I. Bonini, M.M. White, I. Garbus, F.J. Barrantes, Cholesterol depletion activates rapid internalization of submicron-sized acetylcholine receptor domains at the cell membrane, Mol. Membr. Biol. 24 (2007) 1–15, https://doi.org/10.1080/09687860600903387.

[91] C.A. Báez-Pagán, N. Del Hoyo-Rivera, O. Quesada, J.D. Otero-Cruz, J.A. Lasalde-Dominicci, Heterogeneous inhibition in macroscopic current responses of four nicotinic acetylcholine receptor subtypes by cholesterol enrichment, J. Membr. Biol. 249 (2016) 539–549, https://doi.org/10.1007/s00232-016-9896-z.

[92] J.B. Massey, Effect of cholesteryl hemisuccinate on the interfacial properties of phosphatidylcholine bilayers, Biochim. Biophys. Acta, Biomembr. 1415 (1998) 193–204, https://doi.org/10.1016/s0005-2736(98)00194-1.

[93] G. Zhang, H. Liu, L. Yang, Y.G. Zhong, Y.Z. Zheng, Influence of membrane physical state on the lysosomal proton permeability, Membrane. Biol. 175 (2000) 53–62, https://doi.org/10.1007/s002320001054.

[94] W.X. Ding, X.R. Qi, P. Li, Y. Maitani, T. Nagai, Cholesteryl hemisuccinate as a membrane stabilizer in dipalmitoylphosphatidylcholine liposomes containing saikosaponin-d, Int. J. Pharm. 300 (2005) 38–47, https://doi.org/10.1016/j.ijpharm.2005.05.005.

[95] M. Jafurulla, A. Nalli, A. Chattopadhyay, Membrane cholesterol oxidation in live cells enhances the function of serotonin1A receptors, Chem. Phys. Lipids 203 (2017) 71–77, https://doi.org/10.1016/j.chemphyslip.2017.01.005.

[96] X. Chen, D.E. Wolfgang, N.S. Sampson, Use of the parallax-quench method to determine the position of the active-site loop of cholesterol oxidase in lipid bilayers, Biochemistry 39 (2000) 13383–13389, https://doi.org/10.1021/bi001407j.

[97] C. Bouzat, S.M. Sine, Nicotinic acetylcholine receptors at the single-channel level, Br. J. Pharmacol. 175 (2018) 1789–1804, https://doi.org/10.1111/bph.13770.

[98] V. Bermúdez, S.S. Antollini, G.A. Fernández Nievas, M.I. Aveldaño, F.J. Barrantes, Partition profile of the nicotinic acetylcholine receptor in lipid domains upon reconstitution, J. Lipid Res. 51 (2010) 2629–2641, https://doi.org/10.1042/BC20110018.

Membrane lipid organization and nicotinic acetylcholine receptor function: a two-way physiological relationship

C. Fabiani[a], V.N. Georgiev[b], D.A. Peñalva[a], L. Sigaut[c], L. Pietrasanta[c,d], J. Corradi[a], R. Dimova[b], S.S Antollini[a,*]

[a]Instituto de Investigaciones Bioquímicas de Bahía Blanca CONICET-UNS, Departamento de Biología, Bioquímica y Farmacia, Universidad Nacional del Sur, Bahía Blanca, Argentina.

[b]Max Planck Institute of Colloids and Interfaces, Science Park Golm, Potsdam, 14476, Germany.

[c]Departamento de Física, Instituto de Física de Buenos Aires (IFIBA), CONICET-UBA, Facultad de Ciencias Exactas y Naturales, Universidad de Buenos Aires, Buenos Aires, Argentina.

[d]Centro de Microscopías Avanzadas, Facultad de Ciencias Exactas y Naturales, Universidad de Buenos Aires, Buenos Aires, Argentina. ***** Corresponding author.
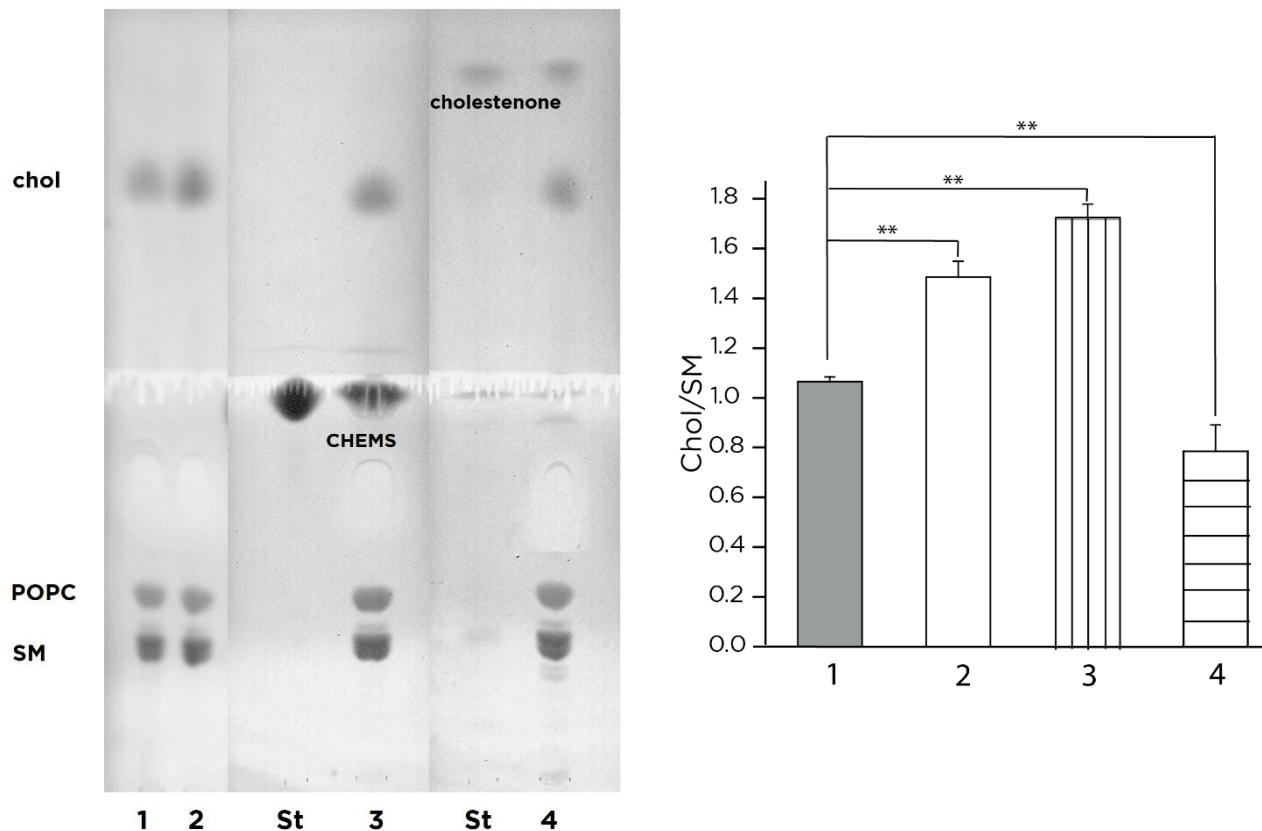
Figure 1 Suppl.

Figure S1. Final lipid composition of LUVs containing POPC:Chol:bSM (1:1:1) after different treatments. *Left)* Representative TLC of lipids extracts. *Right)* Chol/SM ratio of each condition. Each column represents the average ± SD of the total number of samples of each condition (n=3). ** denote highly significant differences (p<0.01) between the control situation and each condition.

        1. POPC:SM:Chol (1:1:1 molar ratio). Control situation.

        2. POPC:SM:Chol (1:1:1 molar ratio) + Chol.

        3. POPC:SM:Chol (1:1:1 molar ratio) + CHEMS.

        4. POPC:SM:Chol (1:1:1 molar ratio) + ChOx.

	Free-protein LUVs			Membranes
	anisotropy		Laurdan GP	Laurdan GP
	DPH	TMA-DPH		
Control	0.2851 ± 0.001	0.3254 ± 0.001	0.3455 ± 0.010	0.4651 ± 0.004
+ Chol	0.2669 ± 0.001	0.3269 ± 0.001	0.3055 ± 0.013	0.4565 ± 0.009
+ CHEMS	0.3220 ± 0.003**	0.3811 ± 0.001**	0.4081 ± 0.002**	0.5052 ± 0.004**
+ ChOx	0.2853 ± 0.002	0.3288 ± 0.002	0.3335 ± 0.006	0.4645 ± 0.001

Table S1. DPH and TMA-DPH anisotropy and Laurdan GP values obtained from free-protein LUVS composed of POPC:Chol:bSM (1:1:1) and from nAChR-rich membranes from T. *californica* before and after the different treatments. Measurements were performed at 25 °C. Statistically significant differences (**, $p<0.01$) compared to the control condition.
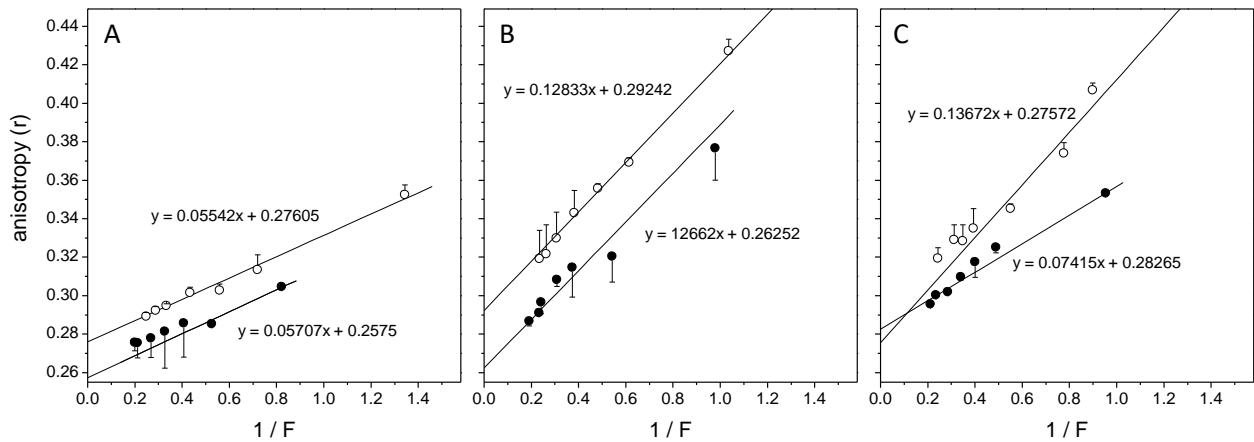
Figure 2 Suppl.

Figure S2. Anisotropy of the fluorescence probes DPH (●) and TMA-DPH (o) in the presence of increasing concentrations of TNBS, a polar-fluorescence quencher. **a**) Control condition, corresponding to LUVs of POPC:Chol:bSM (1:1:1), **b**) POPC:Chol:bSM (1:1:1) + Chol, **c)** POPC:Chol:bSM (1:1:1) + CHEMS. Equations are shown for each condition. Each point corresponds to the mean value ± SD, n=3.
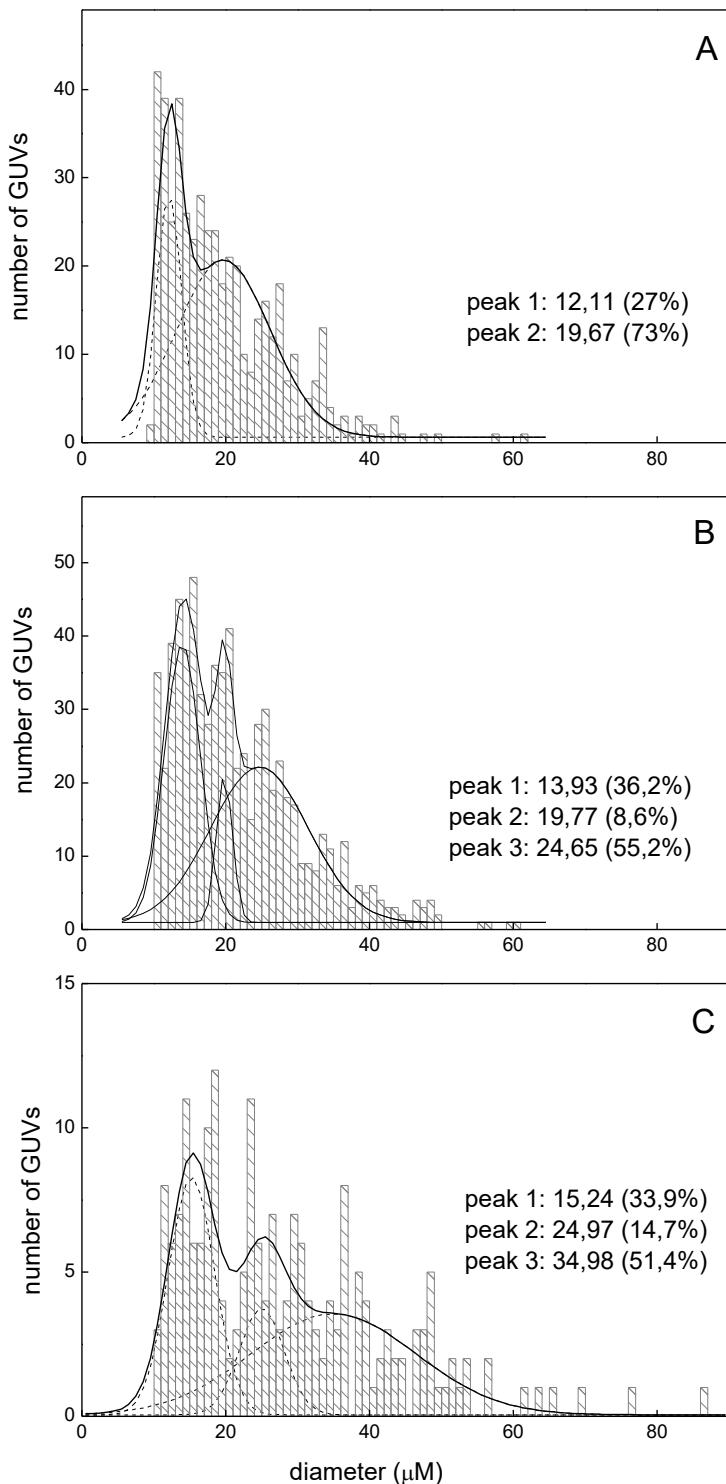
Figure 3 suppl.

Figure S3. Diameter histograms of GUVs made with A) POPC:Chol: SM (1:1:1), B) POPC:Chol:SM (1:2:1), and C) POPC:Chol:SM:CHEMS (1:1:1:1).   Each GUV diameter was measured with the Zen Lite program. For each condition, at least 200 GUVs greater than 10 μm of diameter were considered.
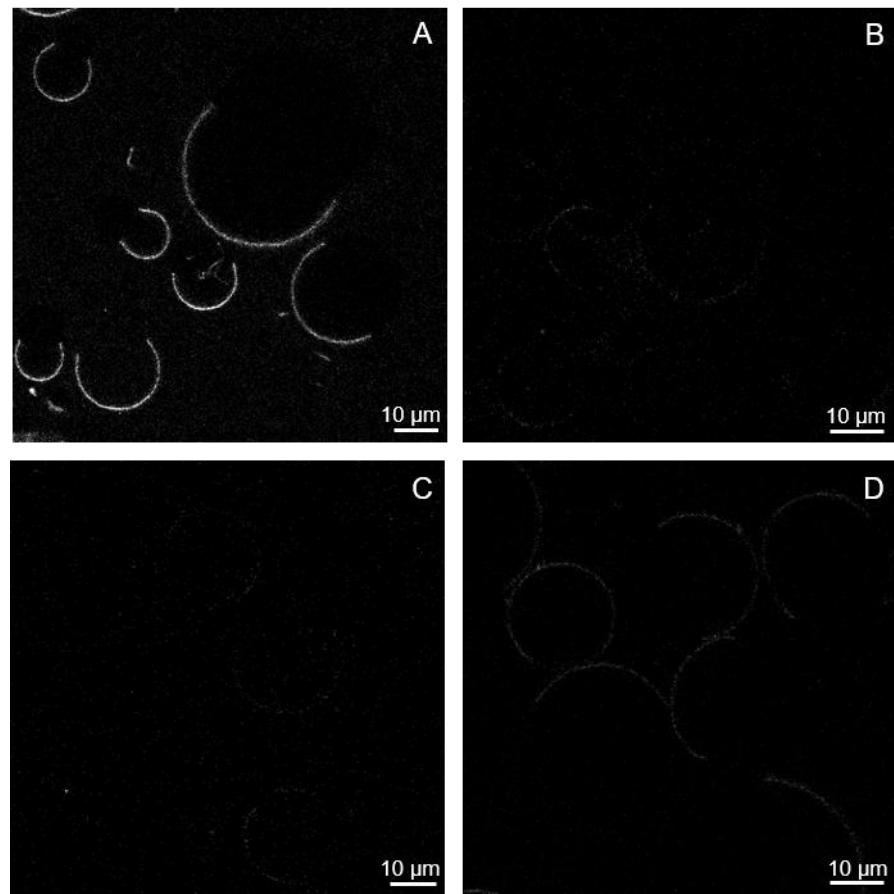
Figure 4 suppl.

Figure S4. Microscopy of Giant Unilamellar Vesicles (GUVs) from the coumarin channel. A) DOPC:Chol:eSM + γTM4 labeled with DiI- C18 and coumarin. B) DOPC:Chol:eSM (1:1:1) labeled with DiI-C18, C) DOPC:Chol:eSM (1:1:1) + γTM4 labeled with DiI-C18 and D) DOPC:Chol:eSM (1:1:1) labeled with DiI-C18 and coumarin. A greater fluorescence intensity is observed in A.